

# Heavy Meson Semileptonic Form Factors from Lattice Quantum Chromodynamics

Euan McLean

*Supervised by Prof. Christine Davies*

*Submitted in fulfillment of the requirements for the degree of  
Doctor of Philosophy*

*April 2019*



*The University of Glasgow  
College of Science and Engineering*



---

**Declaration of originality**

This thesis is my own work, except where explicit attribution to others is made. In particular Chapters ... are based on the following publications:

All results and figures presented in these chapters are my own, except for ...

---



## **Acknowledgments**

I claim sole credit for everything in this thesis.



# Contents

<b>1</b>	<b>Introduction</b>	<b>1</b>
<b>2</b>	<b>Motivation &amp; Tools from the Continuum</b>	<b>3</b>
2.1	Testing the Standard Model . . . . .	3
2.2	Flavour-Changing Charged Currents . . . . .	5
2.2.1	The CKM Matrix . . . . .	7
2.2.2	Weak Decays . . . . .	10
2.2.3	$b \rightarrow c$ Transitions and $ V_{cb} $ . . . . .	14
2.2.4	Flavour Anomalies & Lepton Flavour Violation . . . . .	16
2.3	Strong Interaction Physics . . . . .	19
2.3.1	Quantum Chromodynamics . . . . .	19
2.3.2	Chiral Symmetry . . . . .	21
2.4	Heavy Quark Physics . . . . .	23
2.4.1	HQET . . . . .	23
2.4.2	NRQCD . . . . .	27
<b>3</b>	<b>Lattice Quantum Chromodynamics</b>	<b>29</b>
3.1	Lattice Gauge Fields . . . . .	30
3.1.1	The Gauge Action . . . . .	33
3.1.2	Symmanzik Improvements of the Gauge Action . . . . .	34
3.2	Lattice Fermions . . . . .	36
3.2.1	The Naive Fermion Action & The Doubling Problem . . . . .	37
3.2.2	Staggered Quarks . . . . .	38
3.2.3	Highly Improved Staggered Quarks . . . . .	40
3.3	Heavy Quarks on the Lattice . . . . .	41
3.3.1	Heavy HISQ . . . . .	43
3.3.2	Lattice NRQCD . . . . .	43
<b>4</b>	<b>Lattice Calculations</b>	<b>47</b>
4.1	Evaluating Lattice Correlation Functions . . . . .	47
4.1.1	Generation of Gauge Ensembles . . . . .	48
4.1.2	Dirac Operator Inversion . . . . .	52
4.1.3	Staggered Correlation Functions . . . . .	54

4.2	Analysis of Correlation Functions . . . . .	57
4.2.1	Fitting Correlation Functions . . . . .	57
4.2.2	Signal Degredation . . . . .	60
4.3	Renormalization of Currents . . . . .	61
<b>5</b>	<b><i>b</i>-Physics from Lattice NRQCD</b>	<b>63</b>
5.1	$B_{(s)} \rightarrow D_{(s)} l \nu$ Form Factors . . . . .	63
5.1.1	Calculation Setup . . . . .	63
5.1.2	Results . . . . .	63
5.1.3	The Subleading Current Problem . . . . .	63
5.2	Nonperturbative Renormalisation . . . . .	63
5.2.1	Relativistic Normalisation of the $b \rightarrow c$ Axial Current . . . . .	63
5.2.2	$b \rightarrow c$ Vector Current Matching to Heavy-HISQ . . . . .	63
<b>6</b>	<b><math>B_s \rightarrow D_s^* l \nu</math> Axial Form Factor at Zero Recoil from Heavy-HISQ</b>	<b>65</b>
6.1	Calculation Setup . . . . .	65
6.2	Results . . . . .	65
6.3	Implications for $B \rightarrow D^* l \nu$ and $ V_{cb} $ . . . . .	65
<b>7</b>	<b><math>B_s \rightarrow D_s l \nu</math> Form Factor at All Physical <math>q^2</math> from Heavy-HISQ</b>	<b>67</b>
7.1	Calculation Setup . . . . .	67
7.2	Results . . . . .	67
7.3	HQET low energy constants . . . . .	67

---

# CHAPTER 1

# Introduction

As the LHC continuously refuses to supply new resonances, the high energy physics community places their hope in the intensity frontier to finally break the standard model. Subtle differences between experimental measurements and standard model predictions are the new rock and roll. As collider experiments collect more data and measurements become more precise, theorists must keep up the pace and improve our predictions. What else but Lattice QCD could answer the call of providing first-principle calculations of non-perturbative quantities?

This thesis focuses on the study of calculating form factors for semileptonic  $b \rightarrow c$  transitions. These transitions occur between hadrons, bound together by QCD. At the confinement scale ( $\sim 1\text{GeV}$ ), perturbation theory breaks down due to asymptotic freedom, and the only sensible option is to compute the path integral directly, i.e., via lattice calculations.

The  $b$  quark is difficult to deal with on the lattice, due to its mass being beyond the momentum cutoff imposed by computationally feasible lattice spacings. I calculate  $b \rightarrow c$  form factors using two approaches to dealing with the heavy  $b$ , one employing a non-relativistic action for the  $b$  (*NRQCD*), and the other relying on heavy quark effective theory to extrapolate upwards to the  $b$  mass (*Heavy-HISQ*). The main take-home from this thesis is the following: **when it comes to semileptonic form factors; NRQCD is on shaky ground, and Heavy-HISQ is an excellent way to live.**

Using NRQCD, I attempted to compute form factors for the  $B_{(s)} \rightarrow D_{(s)} l \nu$  decays. The depletion of the signal/noise ratio in correlation functions featuring high spacial momentum means lattice data for this decay was limited to the high  $q^2$  region.

In NRQCD, flavour-changing current operators are made of an infinite series of terms in powers of the  $b$ -quark velocity  $v$ , each requiring their own normalisation via perturbative matching to continuum QCD. It was discovered during this work that subleading terms in this series, that were originally thought to be negligible, in fact may be an important contribution. Since the perturbative matching calculations for these terms have not been performed, this caused a somewhat insurmountable obstacle for the NRQCD approach to calculating  $b \rightarrow c$  form factors.

The NRQCD approach could in principle be saved by finding non-perturbative normalizations of these large subleading terms in the current. We investigated a way of achieving this by comparing NRQCD lattice data to pre-existing and more reliable Heavy-HISQ lattice data, with limited success.

To sidestep the problems with NRQCD, We focused instead on the Heavy-HISQ approach. With this, we successfully calculated the  $B_s \rightarrow D_s^* l \nu$  axial form factor at zero recoil. This demonstrated the power of heavy-HISQ and layed the groundwork for a study of both  $B_s \rightarrow D_s^* l \nu$  and  $B_s \rightarrow D_s l \nu$  form factors away from zero recoil, which is now underway. We also calculated  $B_s \rightarrow D_s l \nu$  form factors throughout the full physical range of momentum transfer. These studies, when combined with future experimental data of the  $B_s \rightarrow D_s l \nu$  and  $B_s \rightarrow D_s^* l \nu$  decays, will supply new tests of the standard model, and new channels to determining the CKM parameter  $|V_{cb}|$ .

All work reported in this thesis was performed using gluon ensembles courtesy of the MILC collaboration, accounting for dynamical up, down, strange and charm HISQ quarks in the sea. We computed correlation functions using a combination of the MILC code, and HPQCD's NRQCD code.

## CHAPTER 2

# Motivation & Tools from the Continuum

---

In this chapter, we lay out the physics context of this work and some theoretical machinery that was useful in our studies. This section consists of a definition and empirical status of the standard model. Then, we will expand on the details of the specific sector we are interested in - the flavour sector and the CKM matrix.

We will then move onto some lay down some physics machinery used in our work, namely QCD and chiral symmetry, and effective field theories for heavy quarks.

### 2.1 Testing the Standard Model

The Standard Model of Particle Physics (SM) is, so far, the most successful theory for describing fundamental particles and their interactions. It is an effective Yang-Mills quantum field theory. It is most succinctly defined by listing its symmetries, field content, and the irreducible representations (irreps) of the symmetries that those fields transform under.

The symmetries are the following. The Lorentz group  $SO(3, 1)$ , the group of coordinate transformations that leave the Minkowski metric invariant, which can be decomposed into  $SU(2)_l \times SU(2)_r$  (*left-handed* and *right-handed*). We denote an irrep as  $(a, b)$  where  $a$  is the  $\sigma^z$  eigenvalue under  $SU(2)_l$  transforms, and  $b$  is that of  $SU(2)_r$ . Then there are internal local gauge symmetries:

$$SU(3)_C \times SU(2)_L \times U(1)_Y, \quad (2.1)$$

irreps of which we denote with  $(x, y, z)$ , where  $x, y$  are the  $SU(3)_C$  and  $SU(2)_W$  irreps and  $z$  is the charge under  $U(1)_Y$ .

The field content is: gauge bosons for each generator of the above gauge symmetries, each transforming in the adjoint of their corresponding symmetry and in the  $(1/2, 1/2)$  irrep of the Lorentz group, denoted  $B_\mu$ ,  $W_\mu$ ,  $G_\mu$  respectively. There are

6  $SU(2)_L$  doublets in the  $(1/2, 0)$  Lorentz irrep;

$$Q_{1,2,3} = \begin{pmatrix} u_L \\ d_L \end{pmatrix}, \begin{pmatrix} c_L \\ s_L \end{pmatrix}, \begin{pmatrix} t_L \\ b_L \end{pmatrix} , \quad (\mathbf{3}, \mathbf{2}, 1/6) \quad (2.2)$$

$$L_{1,2,3} = \begin{pmatrix} \nu_{e,L} \\ e_L \end{pmatrix}, \begin{pmatrix} \nu_{\mu,L} \\ \mu_L \end{pmatrix}, \begin{pmatrix} \nu_{\tau,L} \\ \tau_L \end{pmatrix} , \quad (\mathbf{1}, \mathbf{2}, -1) \quad (2.3)$$

and 9  $SU(2)_L$  singlets in the  $(0, 1/2)$  Lorentz irrep;

$$u_{1,2,3}^R = u_R, c_R, t_R , \quad (\bar{\mathbf{3}}, \mathbf{1}, 2/3) \quad (2.4)$$

$$d_{1,2,3}^R = d_R, s_R, b_R , \quad (\bar{\mathbf{3}}, \mathbf{1}, -1/3) \quad (2.5)$$

$$e_{1,2,3}^R = e_R, \mu_R, \tau_R , \quad (\mathbf{1}, \mathbf{1}, -1). \quad (2.6)$$

We have also listed the SM gauge irreps next to each definition. There is also in principle a further set of right-handed  $SU(2)_L$  singlets,  $\nu_{1,2,3}^R = (\nu_{e,R}, \nu_{\mu,R}, \nu_{\tau,R})$ , but these are singlets of the entire SM gauge group so in a phenomenological sense very much 'not there'. There is also a Lorentz scalar  $SU(2)_L$  doublet, the Higgs  $H$ , with in gauge irrep  $(\mathbf{1}, \mathbf{2}, 1/2)$  that obtains a vacuum expectation value under  $\sim 200\text{GeV}$  and causes a breaking of the above gauge group to  $SU(3)_C \times U(1)_E$ , where  $U(1)_E$  is the electroweak gauge group mediated by the photon.

There is at present no confirmed evidence of physics beyond the SM (or *new physics* (NP)), besides the presence of neutrino ( $\nu$ ) masses. However, there are a number of problems with the SM that heavily imply that there must be new physics. Among the most famous sources of concern are:

- **Dark Matter & Dark Energy** - an estimated 96% of the content of the universe is dark matter and dark energy, that does not interact with the SM gauge group (only via gravity), so cannot be explained by the SM.
- **Matter/Antimatter Asymmetry** - the SM requires there to be an equal amount of matter and antimatter in the universe, however, we observe a massive dominance of matter over antimatter.
- **Neutrino Oscillations** - different species of neutrinos oscillate into each other over time, there is no SM mechanism to explain this.
- **The Hierarchy Problem** - the SM is 'finely tuned', the chances of the Higgs choosing its current vacuum expectation value is estimated to be one in  $\sim 10^{45}$ .

The central goal of particle physics is currently to pin down evidence against the standard model. Only once we have detailed knowledge of how it breaks down will theorists be able to uniquely determine a new theory of fundamental physics.

There are many promising approaches to achieve this. They are traditionally separated into

- **The Energy Frontier** - explore the highest possible energies reachable with accelerators, directly looking for new physics via the production and identification of new states of matter.
- **The Cosmic Frontier** - use the universe as an experimental laboratory and observatory, taking advantage of naturally occurring events to observe indications of new interactions.
- **The Intensity Frontier** - use intense sources of particles from accelerators, reactors, the sun and the atmosphere to make ultra-precise measurements and find subtle deviations from SM predictions.

The work in this thesis contributes to the third approach. There is a rising tide of more and more SM observables being measured and predicted more and more precisely. It is only a matter of time until one of these observables yields a statistically significant deviation from the SM.

## 2.2 Flavour-Changing Charged Currents

The SM tests relevant to this work are on quark flavour-changing interactions. Here we will detail the parts of the SM relevant to these interactions.

The  $SU(2)_L$  gauge symmetry of the SM is mediated by the vector boson  $W = W^1\tau_1 + W^2\tau_2 + W^3\tau_3$ , where  $\tau_i$  are the three  $SU(2)$  generators acting on the  $SU(2)_L$  doublets defined in the last section. It is convenient to redefine the fields  $W = W^+(\tau_0 + i\tau_1) + W^-(\tau_0 - i\tau_1) + W^3\tau_3$ .  $W^\pm, W^3$  are the stationary states at low energies due to electroweak symmetry breaking.

The part of the SM Lagrangian that describes the coupling of  $W^\pm$  to fermions is given by

$$\mathcal{L}_{\text{FCCC}} = \frac{e}{\sqrt{2}\sin\theta_W} \left( \bar{u}_L^i W^+ d_L^i + \bar{d}_L^i W^- u_L^i + \bar{\nu}_L^i \bar{W}^+ e_L^i + \bar{e}_L^i W^- \nu_L^i \right), \quad (2.7)$$

where  $e$  is the electron charge,  $\theta_W$  is the Weinberg angle (a parameter of the SM), and  $\not{V} = \gamma^\mu V_\mu$  where  $\gamma^\mu$  are members of the Clifford algebra acting on fermion

spin components. To understand the interactions these terms cause we must also consider the mass terms for the fermions:

$$\mathcal{L}_{\text{mass}} = y_{ij}^u \left( \frac{v}{\sqrt{2}} \right) u_L^i u_R^j + y_{ij}^d \left( \frac{v}{\sqrt{2}} \right) d_L^i d_R^j + y_{ij}^e \left( \frac{v}{\sqrt{2}} \right) e_L^i e_R^j. \quad (2.8)$$

These terms come from the coupling of the fermions to the Higgs field, where the Higgs has taken a vacuum expectation value  $v$  at low energies.  $y_{ij}^{u,d,e}$  are the Yukawa matrices, parameterising the coupling of the fermions to the Higgs, consisting of free SM parameters. The absence of right-handed neutrinos forbids an analogous term for neutrinos.

Due to these nondiagonal mass terms, the fundamental fermion fields are not stationary states. To obtain a more useful representation, one rotates the fields to diagonalise these terms

$$\psi_i^L \rightarrow L_{ij}^\psi \psi_j^L, \psi_R^i \rightarrow R_{ij}^\psi \psi_R^j, \quad (2.9)$$

where  $\psi = u, d$  or  $e$ , and we fix  $L_{ij}^\psi, R_{ij}^\psi$  according to

$$y^\psi \left( \frac{v}{\sqrt{2}} \right) = L^\psi M^\psi R^\psi \quad (2.10)$$

where  $M^\psi$  is diagonal. This results in diagonal mass terms, but also has an effect on  $\mathcal{L}_{\text{FCCC}}$ :

$$\mathcal{L}_{\text{FCCC}} = \frac{e}{\sqrt{2} \sin \theta_W} \left( V_{ij} \bar{u}_L^i W^+ d_L^j + V_{ij}^* \bar{d}_L^i W^- u_L^j + \bar{\nu}_L^i W^+ e_L^i + \bar{e}_L^i W^- \nu_L^i \right). \quad (2.11)$$

$V = L^{u\dagger} L^u$  is by construction a unitary matrix ( $V^\dagger V = (L^{d\dagger} L^d)(L^{u\dagger} L^u) = L^d L^{d\dagger} = 1$ ).  $V$  is the famous Cabibbo–Kobayashi–Maskawa (CKM) matrix, consisting of parameters that must be fixed by experiment.

There is no non-diagonal flavour structure in the last two terms because we have redefined the neutrino fields:  $\nu_L \rightarrow L^{e\dagger} \nu_L$ , absorbing the rotation of the  $e_L$  fields. This can be done with impunity due to the lack of neutrino mass terms. While the SM does not include neutrino mass terms, it has in fact been experimentally confirmed that neutrinos have mass. It is however known that these masses are extremely small in comparison to the scales of the SM ( $m_\nu \lesssim 0.05 \text{ eV}$ ). Any lepton flavour-changing effect this could in principle have would be much smaller than the current sensitivity of any experiment, for example,  $\mathcal{B}(\mu \rightarrow \tau \gamma) \simeq 10^{-34}$ .

Another useful redefinition is to collect the left-handed and right-handed fermion fields into Dirac spinors  $\psi$ :

$$\psi = \psi_L + \psi_R, \psi_L = \frac{1}{2} (1 - \gamma^5) \psi, \psi_R = \frac{1}{2} (1 + \gamma^5) \psi \quad (2.12)$$

In terms of Dirac spinors,  $\mathcal{L}_{\text{FCCC}}$  can be written as

$$\mathcal{L}_{\text{FCCC}} = \frac{e}{\sqrt{2} \sin \theta_W} \left( V_{ij} J_\mu^{ij} W^{+\mu} + V_{ij}^* J_\mu^{ij\dagger} W^{-\mu} + L_\mu^{ii} W^{+\mu} + L_\mu^{ii\dagger} W^{-\mu} \right), \quad (2.13)$$

$$L_\mu^{ij} = \frac{1}{2} (\bar{\nu}^i \gamma_\mu e^j - \bar{\nu}^j \gamma_5 \gamma_\mu e^i), \quad (2.14)$$

$$J_\mu^{ij} = \frac{1}{2} (\bar{u}^i \gamma_\mu d^j - \bar{u}^j \gamma_5 \gamma_\mu d^i) \equiv V_\mu^{ij} - A_\mu^{ij}. \quad (2.15)$$

$J_\mu^{ij}$  is known as the Flavour-Changing Charged Current (FCCC). It is often broken up into the *vector* and *axial-vector* components,  $V_\mu$  and  $A_\mu$  respectively, since these two components can be categorised according to their transformations under the Lorentz group.  $V_\mu$  is labelled  $1^+$ , where the 1 represents its total spin, and the + represents its positive parity  $P : V_\mu \rightarrow V_\mu$ .  $A_\mu$  is instead labelled  $1^-$ , due to its negative parity  $P : A_\mu \rightarrow -A_\mu$ .

We can now turn to the physical consequences of  $\mathcal{L}_{\text{FCCC}}$ . The interactions given in this part of the Lagrangian describe a quark changing flavour while emitting a  $W^\pm$  boson. The propensity for flavour  $i$  to decay into another flavour  $j$  is governed in part by energy constraints and in part by the associated CKM element  $V_{ij}$ . These interactions at the quark level mediate meson decays, namely leptonic and semileptonic decays, described in section 2.2.2.

The deviation of  $V_{ij}$  from a unit matrix breaks some of the symmetries of the SM.  $\mathcal{L}_{\text{SM}} - \mathcal{L}_{\text{FCCC}}$  has the property that one can independently rephase each of the quark fields,  $q_i \rightarrow e^{i\theta_i} q_i$ , a global  $U(1)$  symmetry for each quark flavour. This implies, via Noether's theorem, that the number of quarks of each flavour,  $N_i$ , is conserved. However,  $\mathcal{L}_{\text{FCCC}}$  breaks this symmetry  $U(1)^6 \rightarrow U(1)$ , where there is only a remnant symmetry of transforming all flavours by the same phase. Individual quark flavour number is no longer conserved, but overall quark number is.

Since there is no off-diagonal flavour structure for the Leptons, the equivalent global  $U(1)^6$  symmetry for the leptons survives in the SM, and individual lepton flavour number is conserved. This property of the SM is referred to as lepton flavour universality.

### 2.2.1 The CKM Matrix

The exact values of the CKM matrix elements are of interest in the search for new physics. The CKM matrix is unitary by construction, however, if we were to discover that the values we measure experimentally do not combine to produce a unitary matrix, this would be evidence that the elements we are measuring, in fact,

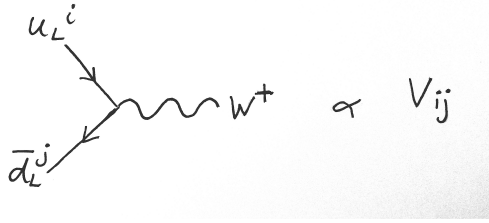


Figure 2.1: The flavour-changing charged current vertex.

compose a submatrix of a unitary matrix larger than  $3 \times 3$ . This would imply the presence of further, heavier quark generations.

The CKM contains 3 real parameters and 1 complex phase. There is only one complex phase since we can freely redefine the phases of the quark fields in order to absorb the majority of the phases in the CKM. A common parameterisation is

$$V = \begin{pmatrix} 1 & 0 & 0 \\ 0 & \cos \theta_{23} & \sin \theta_{23} \\ 0 & -\sin \theta_{23} & \cos \theta_{23} \end{pmatrix} \begin{pmatrix} 1 & 0 & \sin \theta_{12} e^{i\delta} \\ 0 & 1 & 0 \\ -\sin \theta_{13} e^{i\delta} & 0 & \cos \theta_{13} \end{pmatrix} \begin{pmatrix} \cos \theta_{12} & \sin \theta_{12} & 0 \\ -\sin \theta_{12} & \cos \theta_{12} & 0 \\ 0 & 0 & 1 \end{pmatrix}. \quad (2.16)$$

A useful parameterisation for understanding the relative sizes of the CKM elements is due to Wolfenstein. Define the Wolfenstein parameter  $\lambda = \sin \theta_{12}$ , which is known experimentally to be around  $\lambda \simeq 0.22$ . Then  $\cos \theta_{12} = \sqrt{1 - \sin^2 \theta_{12}} = \sqrt{1 - \theta^2} \simeq 1 - \lambda^2/2$ . Observing then that  $\sin \theta_{23} \sim 0.04 \simeq \lambda^2$  and  $\sin \theta_{13} \sim 0.004 \simeq \lambda^3/3$ , we can write the matrix as

$$V \simeq \begin{pmatrix} 1 - \frac{1}{2}\lambda^2 & \lambda & \frac{1}{3}\lambda^3 e^{i\delta} \\ -\lambda & 1 - \frac{1}{2}\lambda^2 & \lambda^2 \\ \lambda^3(1 - \frac{1}{3}e^{i\delta}) & -\lambda^2 & 1 \end{pmatrix} = \begin{pmatrix} \mathcal{O}(1) & \mathcal{O}(\lambda) & \mathcal{O}(\lambda^3) \\ \mathcal{O}(\lambda) & \mathcal{O}(1) & \mathcal{O}(\lambda^2) \\ \mathcal{O}(\lambda^3) & \mathcal{O}(\lambda^2) & \mathcal{O}(1) \end{pmatrix} \quad (2.17)$$

There is a clear hierarchy between the values - the CKM matrix is close to the unit matrix. Inter-generational mixing is dominant, dropping from second to first generation is suppressed by  $\lambda$ , dropping from third to second by  $\lambda^2$ , and dropping from third to first by  $\lambda^3$ . The SM supplies no compelling explanation of why this hierarchy exists, it is expected that new physics beyond the SM will supply some natural explanation.

The assumption of unitarity in  $V$ ,

$$V_{ji}^* V_{jk} = \delta_{ik}, \quad (2.18)$$

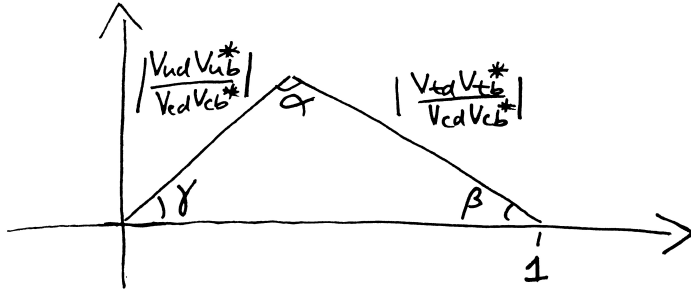


Figure 2.2: A sketch of the unitarity triangle.

imposes 9 constraints on the CKM elements. Each of these constraints gives a test of the SM, if one of these constraints is found to be violated, this represents evidence of new physics. The most studied constraint is given by taking  $i = 3, k = 1$ ;

$$\frac{V_{ud} V_{ub}^*}{V_{cd} V_{cb}^*} + \frac{V_{td} V_{tb}^*}{V_{cd} V_{cb}^*} + 1 = 0. \quad (2.19)$$

This can be visualized as a triangle (known as the *unitarity triangle*) on the complex plane, as shown in figure 2.2.

For unitarity, the triangle must close, in other words,  $\alpha + \beta + \gamma = \pi/2$ . Hence to test the CKM unitarity experimentalists measure these angles

$$\alpha = \arg\left(-\frac{V_{td} V_{tb}^*}{V_{ud} V_{ub}^*}\right), \beta = \arg\left(-\frac{V_{cd} V_{cb}^*}{V_{td} V_{tb}^*}\right), \gamma = \arg\left(-\frac{V_{ud} V_{ub}^*}{V_{cd} V_{cb}^*}\right). \quad (2.20)$$

The unitarity triangle also contains information about CP-violation from flavour-changing charged currents. The so-called Jarlskog invariant,  $J = \sin \theta_{12} \sin \theta_{23} \sin \theta_{31} \cos \theta_{12} \cos \theta_{23} \cos \theta_{31}^2 \sin \delta$ , a measure of CP-violation, is proportional to the area enclosed by the triangle.

The most recent PDG update [1] reports the following averages for the measurements of CKM elements;

$$|V| = \begin{pmatrix} 0.97446 \pm 0.00010 & 0.22452 \pm 0.00044 & 0.00365 \pm 0.00012 \\ 0.22438 \pm 0.00044 & 0.97359^{+0.00010}_{-0.00011} & 0.04214 \pm 0.00076 \\ 0.00896^{+0.00024}_{-0.00023} & 0.04133 \pm 0.00074 & 0.999105 \pm 0.000032 \end{pmatrix}. \quad (2.21)$$

The averages given here are consistent with unitarity in all available tests. The angles of the unitarity triangle currently satisfy  $\alpha + \beta + \gamma = (180 \pm 7)^\circ$ . Increasing the precision of CKM determinations are necessary to provide more stringent tests of CKM unitarity.

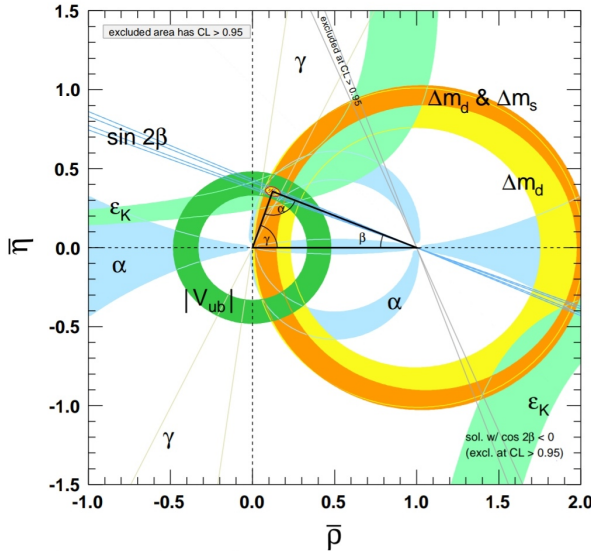


Figure 2.3: Exclusion regions for the vertices of the CKM triangle from various measurements, courtesy of the most recent PDG update [1].

### 2.2.2 Weak Decays

We now move on to the methods of determining CKM elements. At the confinement scale ( $\sim 1\text{GeV}$  and below), quarks are confined by QCD in hadrons. At these energies, the dynamics of quarks are only experimentally accessible by probing the dynamics of hadrons. CKM matrix elements are determined by studying hadron decays.

First a word on hadrons. Hadrons are broadly categorized into mesons (charged with one valence quark and one valence antiquark) and baryons (three valence quarks). The entirety of this thesis is concerned with mesons. Mesons are categorized in terms of the flavours they are charged under and their representations under the Lorentz group. We use the same notation as for the quantum numbers of the weak currents;  $L^\pm$  where  $L$  denotes spin and  $\pm$  denotes parity. In this thesis, we are concerned mostly with pseudoscalar ( $0^-$ ) and vector ( $1^-$ ) mesons.

Weak decays of mesons are categorized according to the final products:

- **Leptonic:**  $\text{meson} \rightarrow \text{leptons}$ .
- **Semileptonic:**  $\text{meson} \rightarrow \text{meson} + \text{leptons}$ .
- **Hadronic:**  $\text{meson} \rightarrow \text{mesons}$ .
- **Oscillation:**  $\text{meson} \rightarrow \text{meson}$ .

All of these types of decay are dependent on CKM elements so can in principle

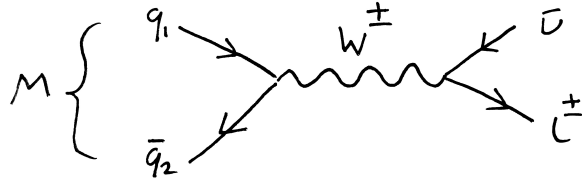


Figure 2.4: Leptonic decay of meson  $M$  at tree level in the electroweak coupling.

to be used for studying them. We are most interested in the first two, leptonic and semileptonic, so will give detail of such decays here.

Fig. 2.4 shows a generic leptonic decay at tree level (in electroweak coupling, virtual quark and gluon lines are implicit). The corresponding amplitude is given by

$$\mathcal{M} = \left( \frac{ie}{\sqrt{2} \sin \theta_W} \right) V_{q_1 q_2} \langle l \bar{\nu} | L_\mu^l D_W^{\mu\nu} J_\nu^{q_1 q_2} | M \rangle, \quad (2.22)$$

where  $D_W$  is a free  $W^{+-}$  propagator,  $|M\rangle$  is the ground state of the meson  $M$ , and  $|l \bar{\nu}\rangle$  is a lepton-antineutrino state. We are using the notation  $L_\mu^l = L_\mu^{kk}$ , where  $l$  indexes the  $k$ th charged lepton. If the momentum of the meson,  $p^2$ , is much smaller than the  $W$  mass squared, one can integrate out the dynamics of the  $W$  to move into the Fermi effective theory [2];

$$\begin{aligned} \left( \frac{ie}{\sqrt{2} \sin \theta_W} \right)^2 D_W^{\mu\nu}(p^2) &= \left( \frac{ie}{\sqrt{2} \sin \theta_W} \right)^2 \left( \frac{-ig^{\mu\nu}}{p^2 - M_W^2} \right) \\ &= \underbrace{\frac{i}{M_W^2} \left( \frac{ie}{\sqrt{2} \sin \theta_W} \right)^2 g^{\mu\nu}}_{\equiv -2\sqrt{2}G_F} + \mathcal{O}\left(\frac{p^2}{M_W^4}\right). \end{aligned} \quad (2.23)$$

Then  $\mathcal{M}$  can be factorised;

$$\mathcal{M} \simeq -2\sqrt{2}V_{q_1 q_2} \langle l \bar{\nu} | L_\mu^l | \Omega \rangle \langle \Omega | J_\mu^{q_1 q_2} | M \rangle. \quad (2.24)$$

$\langle \Omega | J_\mu^{q_1 q_2} | M \rangle$  is a non-perturbative quantity, since it concerns the transitions of a strongly coupled bound state (QCD at the confinement scale). We know that it has a lorentz index  $\mu$ , and the only Lorentz vector in the system is the meson's 4-momentum  $p_\mu$ . So we define

$$\langle \Omega | J_{q_1 q_2}^\mu | M \rangle = p^\mu f_M, \quad (2.25)$$

where  $f_M$  is a Lorentz invariant known as the *decay constant* of the meson  $M$ , and encodes all non-perturbative information in the amplitude.

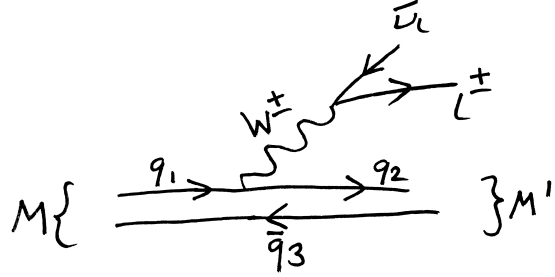


Figure 2.5: Semileptonic decay,  $M \rightarrow M' l \bar{\nu}$ , at tree level in electroweak coupling.

By taking the modulus squared of  $\mathcal{M}$ , and integrating over all allowed momenta of the final state, one finds the decay rate of the process;

$$\Gamma(M \rightarrow l \bar{\nu}) = \frac{G_F^2}{8\pi} f_M^2 m_l^2 M_M \left(1 - \frac{m_l}{M_M^2}\right)^2 |V_{q_1 q_2}|^2, \quad (2.26)$$

In order to find  $|V_{q_1 q_2}|$ , one requires both a measurement of  $\Gamma(M \rightarrow l \bar{\nu})$ , and a value for  $f_M$ .  $f_M$  can be computed in a Lattice QCD calculation.

A similar story accompanies semileptonic decays. At tree level in the electroweak coupling, a typical semileptonic decay is depicted in fig. 2.8. The amplitude is given by

$$\begin{aligned} \mathcal{M} &= \left( \frac{ie}{\sqrt{2} \sin \theta_W} \right) V_{q_1 q_2} \langle M', l \bar{\nu} | J_\mu^{q_1 q_2} D_W^{\mu\nu} L_\nu^l | M \rangle \\ &\simeq -2\sqrt{2} G_F V_{q_1 q_2} \langle M', l \bar{\nu} | J_\mu^{q_1 q_2} L^l{}^\mu | M \rangle \\ &\simeq -2\sqrt{2} G_F V_{q_1 q_2} \langle l \bar{\nu} | L^l{}^\mu | \Omega \rangle \langle M' | J_\mu^{q_1 q_2} | M \rangle, \end{aligned} \quad (2.27)$$

where on the second line we have integrated out the  $W$  propagator in using the same expansion as in the leptonic case, and on the third line we have factorised the QCD part from the electroweak part. The matrix element  $\langle M' | J_\mu^{q_1 q_2} | M \rangle$  is a non-perturbative quantity. Unlike in the previous case, there are a number of ways one can choose to parameterise this matrix element, and appropriate choices vary depending on the quantum numbers of  $M$  and  $M'$ . Of interest to us are the cases where  $M$  is a pseudoscalar meson  $0^-$ , and  $M'$  is either pseudoscalar or vector  $1^-$ .

In the **pseudoscalar**→**pseudoscalar** case, only the vector component of the current survives in the matrix element,  $\langle M' | J_\mu^{q_1 q_2} | M \rangle = \langle M' | V_\mu^{q_1 q_2} | M \rangle$ .  $\langle M' | A_\mu^{q_1 q_2} | M \rangle$  vanishes since this does not respect the parity invariance of QCD. The most popular parameterisation of  $\langle M' | V_\mu^{q_1 q_2} | M \rangle$  is

$$\langle M' | V_\mu^{q_1 q_2} | M \rangle = f_+(q^2) \left[ P_\mu + p_\mu - \frac{M^2 - m^2}{q^2} q_\mu \right] + f_0(q^2) \frac{M^2 - m^2}{q^2} q_\mu. \quad (2.28)$$

$M, P_\mu$  are the  $M$ -meson mass and momentum,  $m, p_\mu$  are the  $M'$ -meson mass and momentum.  $f_0(q^2)$  and  $f_+(q^2)$ , known as the scalar and vector form factors, encoding all non-perturbative information. We now have non-perturbative functions of  $q^2$  rather than a single number.  $q^2 = (P - p)^2$ , the momentum carried away from the meson by the  $W$ , has an allowed range of values if the final states are on-shell;

$$m_l^2 \leq q^2 \leq (M - m)^2. \quad (2.29)$$

By integrating  $|\mathcal{M}|^2$  over all final lepton and neutrino momenta, one finds a differential decay rate,

$$\begin{aligned} \frac{d\Gamma}{dq^2}(M \rightarrow M' l \bar{\nu}) = & \eta_{\text{EW}} \frac{G_F^2 |V_{q_1 q_2}|^2}{24\pi^3 M^2} \left(1 - \frac{m_l^2}{q^2}\right)^2 |\mathbf{p}| \times \\ & \left[ \left(1 + \frac{m_l^2}{2q^2}\right) M^2 |\mathbf{p}|^2 f_+^2(q^2) + \frac{3m_l^2}{8q^2} (M^2 - m^2)^2 f_0^2(q^2) \right]. \end{aligned} \quad (2.30)$$

$\eta_{\text{EW}}$  is the electroweak correction, due to diagrams involving an exchange of a photon or a  $Z$ -boson alongside the  $W$  between the meson and leptons.  $\mathbf{p}$  is the final meson state ( $M'$ ) spacial momentum. Once again, to deduce  $|V_{q_1 q_2}|$ , one requires both the decay rates  $d\Gamma/dq^2$ , and the form factors  $f_0(q^2), f_+(q^2)$ . To precisely determine the form factors requires a Lattice QCD calculation.

In the **pseudoscalar**→**vector** case, both the vector and axial-vector components of the current survive in the matrix element. A common choice of parameterisation is

$$\langle M'(\epsilon) | V_{q_1 q_2}^\mu | M \rangle = i\sqrt{Mm} h_V^s(w) \epsilon_{\mu\nu\alpha\beta} \epsilon^{*\nu} v'^\alpha v^\beta, \quad (2.31)$$

$$\langle M'(\epsilon) | A_{q_1 q_2}^\mu | M \rangle = \sqrt{Mm} [h_{A_1}^s(w)(w+1)\epsilon_\mu^* -$$

$$h_{A_2}^s(w) \epsilon^* \cdot v v_\mu - h_{A_3}^s(w) \epsilon^* \cdot v v'^\mu].$$

$v = P/M$  and  $v' = p/m$  are the 4-velocities of  $M$  and  $M'$  respectively.  $\epsilon$  is the polarization of the vector meson  $M'$ .  $w = v \cdot v'$  is known as the recoil parameter, this is an alternative to  $q^2$  often used in heavy quark effective theory.  $h_V(w), h_{A_0}(w), h_{A_1}(w)$ , and  $h_{A_2}(w)$  are the form factors accounting for the non-perturbative physics. The decay rate is given by

$$\frac{d\Gamma}{dw}(M \rightarrow M' l \bar{\nu}) = \frac{G_F^2 m^3 |\eta_{\text{EW}} V_{q_1 q_2}|^2}{4\pi^3} (M - m)^2 \sqrt{w^2 - 1} \chi(w) |\mathcal{F}(w)|^2, \quad (2.33)$$

where  $\mathcal{F}(w)$  is a linear combination of the form factors and  $\chi(w)$  is a known function of  $w$  (both given in e.g. [3]).

At the zero recoil point, where  $q^2$  is maximized at  $q_{\max}^2 = (M - m)^2$ , (corresponding to  $w = 1$ ), a single form factor contributes

$$\mathcal{F}(1) = h_{A_1}(1). \quad (2.34)$$

However the differential decay rate vanishes at  $w = 1$ . A common approach to determine  $|V_{q_1 q_2}|$ , for example used to find  $|V_{cb}|$  via the  $B \rightarrow D^* l \bar{\nu}$  decay, is to find  $|\mathcal{F}(1)V_{cb}|^2$  at zero recoil by extrapolating from experimental data at non-zero recoil, and combining this with a lattice QCD determination of  $h_{A_1}(1)$ .

### 2.2.3 $b \rightarrow c$ Transitions and $|V_{cb}|$

The family of weak decays that have attracted the most attention are decays of  $B$  mesons (pseudoscalar mesons containing a valence  $b$  and  $u, d, s$  or  $c$  quark).  $B$  mesons decay into a rich variety of decay products. It is the heaviest quark flavour that can be found in hadrons (the only heavier quark, the top quark, has a mass far above the confinement scale, so does not feature as a valence quark in hadrons).

The  $b$  can decay into either a  $c$  or a  $u$  quark via the flavour changing charged current. In this thesis we are interested in the  $b \rightarrow c$  transition, with an amplitude proportional to the CKM element  $|V_{cb}|$ . In this section, we give a brief overview of how this is calculated and the value's current status.

$B$  meson decays can be measured in a number of experiments. There are two so-called  $b$ -factories, the Belle (II) experiment at the KEKB collider in Japan, and the BaBar experiment at the PEP-II collider at SLAC laboratory in the US. These are  $e^+ e^-$  colliders, that collide with an energy tuned to the mass of the  $\Upsilon(4s)$ , an excited state of the  $\Upsilon$  meson (a  $1^-$  state with  $\bar{b}b$  valence quarks). The  $\Upsilon(4s)$  has a large branching fraction into a  $B\bar{B}$  pair, the decays of these can be measured with large statistics.  $B$  decays can also be measured in proton colliders, like at the LHCb experiment at CERN. Measurements from LHCb have poorer statistics but cover a larger range of the phase space of final states, due to the variance of momenta in the initial state protons.

So far 3 approaches to determining  $|V_{cb}|$  have been carried out:

- $B \rightarrow D^* l \bar{\nu}$  decay rate measurements are extrapolated to zero recoil to determine  $|V_{cb} h_{A_1}(1)|$ . Then dividing out  $h_{A_1}(1)$  from a Lattice calculation, one finds  $|V_{cb}|$ .
- $B \rightarrow D l \bar{\nu}$  decay rates are measured throughout  $q^2$ , and combined with  $f_0(q^2)$  and  $f_+(q^2)$  from lattice calculations.

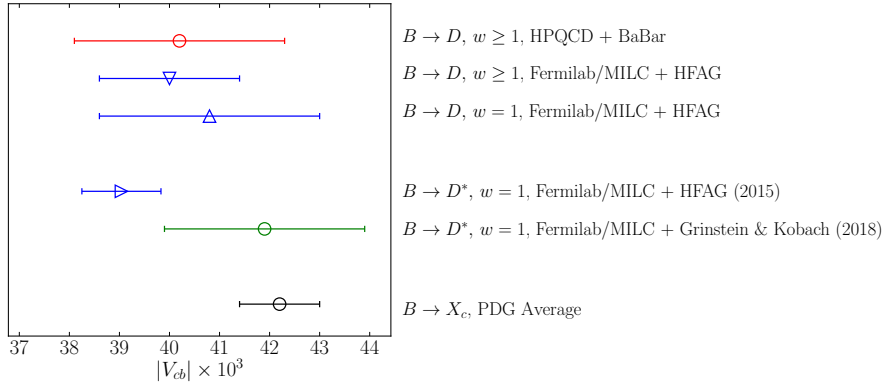


Figure 2.6: Different determinations of  $|V_{cb}|$ . Points labelled  $w = 1$  are determinations from extrapolating measurements of decay rates to the zero recoil point, and combining them with a lattice determination of the form factor at zero recoil. Points labelled  $w \geq 1$  are results from using a combination of both branching fractions and lattice form factors through some range of  $w$ . The first name mentioned in the labels give the source of the lattice form factors, and the second gives the source of the experimental data (e.g. the HPQCD+BaBar point used form factors from the HPQCD collaboration and data from the BaBar experiment). The highest point is from [6], the second and third highest from [7], fourth from [8], fifth from [9]. The bottom point is from the PDG [1], using data from the ALPEPH [10], Belle [11], BaBar [12, 13], and CLEO [14] experiments.

- $B \rightarrow X_c l \bar{\nu}$  decay rates are measured (where  $X_c$  is all possible charmed final state mesons), this is used to constrain elements in the operator product expansion, a method first devised in [4, 5].

The first two are referred to as *exclusive* and the third *inclusive*. A selection of the most accurate examples of each method of determination is given in figure 2.6.

This figure tells a story of the recent history of  $|V_{cb}|$ . Determinations from  $B \rightarrow D l \bar{\nu}$  have been consistent but not as precise as via the other two methods. Until recently, there was a  $3\sigma$  tension between determinations from the  $B \rightarrow D^* l \bar{\nu}$  decay and inclusive decays. This was on its way to being resolved when concern was raised about the method of extrapolating experimental data for  $B \rightarrow D^* l \bar{\nu}$  decay rates to the zero recoil point ( $w = 1$ ).

The Heavy Flavour Averaging Group HFAG (Now HFLAV) determination of  $|V_{cb} h_{A_1}(1)|$  in 2015 parameterised the form factors in the extrapolation using the CLN parameterisation (defined in section ?). It has become clear that the con-

straints the CLN parameterisation imposes on the form factors are not justified. In [9, 15], the results of an extrapolation using the CLN parameterisation were compared to results from a more general, model-independent parameterisation, the BGL parameterisation. It was found that they differed by  $3.5\sigma$ . Since the BGL makes fewer assumptions, one may consider this the more reliable result.

The  $|V_{cb}|$  result using BGL to extrapolate the decay rates is given in the green point on fig. 2.6. Hence, if this work is to be trusted, the long-standing  $|V_{cb}|$  tension has been resolved.

There are however a number of other reasons to be interested in studying  $|V_{cb}|$ , namely improving its precision. It is currently the least precisely determined element of the CKM matrix. It constrains one side of the unitarity triangle via the ratio  $|V_{ub}|/|V_{cb}|$ , so it is the bottleneck for precise tests of CKM unitarity. It is also a dominant uncertainty in the determination of the  $CP$ -violation parameter  $\epsilon_K$  (that is currently at tension between the SM and experiment, see for example [16] where a  $4\sigma$  tension is reported).

#### 2.2.4 Flavour Anomalies & Lepton Flavour Violation

The SM can be tested by studying semileptonic decays more directly, without any consideration of CKM elements. CKM-independent observables can be constructed by taking ratios of branching fractions for decays with common CKM dependence. Then, form factors from lattice QCD can be used to form pure SM predictions of these ratios, and compared to purely experimental measurements. Such comparisons have uncovered a number of tensions between the SM and experiment.

The ratios are defined by

$$R_{X_q} = \frac{\Gamma(B_q \rightarrow X_q \tau \nu_\tau)}{\frac{1}{2} [\Gamma(B_q \rightarrow X_q e \nu_e) + \Gamma(B_q \rightarrow X_q \mu \nu_\mu)]}, \quad (2.35)$$

where  $X_q$  is any meson with valence quark content  $x\bar{q}$ . The numerator and denominator will have the same power of  $|V_{bx}|$ , so cancel in the ratio.

There is currently tension between SM and experiment in  $R_D$  and  $R_{D^*}$ .

$$R_{D^*}|_{\text{exp}} = 0.306(13)_{\text{stat}}(07)_{\text{sys}} , \quad R_{D^*}|_{\text{SM}} = 0.252(3) \quad (2.36)$$

$$R_D|_{\text{exp}} = 0.407(39)_{\text{stat}}(24)_{\text{sys}} , \quad R_D|_{\text{SM}} = 0.300(8). \quad (2.37)$$

The experimental values are the HFLAV averages, from BaBar [17, 18], Belle [19–22], and LHCb [23–25] data. The  $R_{D^*}|_{\text{SM}}$  number is from [26].  $R_D|_{\text{SM}}$  is an average of Lattice results from the HPQCD [6] and FNAL/MILC collaborations [7].

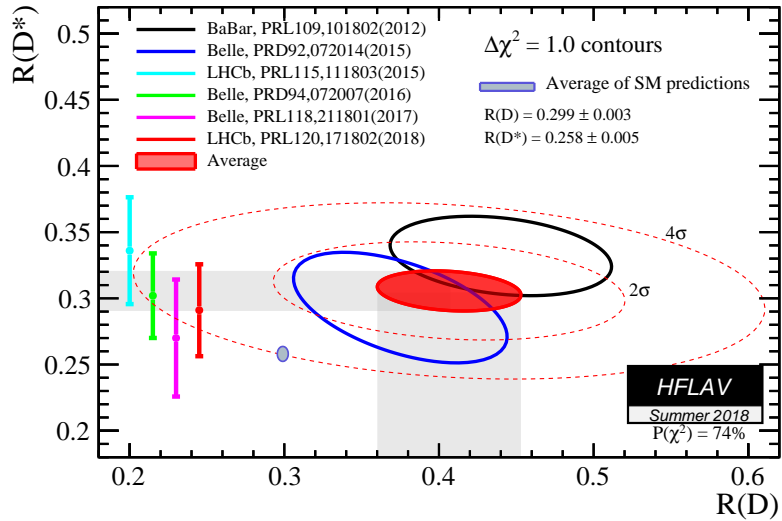


Figure 2.7:  $R(D^{(*)})$  determinations from SM and measurement [27]

A joint analysis of  $R_D$  and  $R_{D^*}$  by HFLAV shows the combined tension to have a significance of  $4.0\sigma$  (see fig. 2.7). Clearly more precise experimental results are necessary to either confirm or dismiss this anomaly. While the SM values are currently much more precise than the experimental ones, further work on the theoretical results is necessary. More independent calculations are required to make the SM numbers more robust, so that, if this tension ever hits  $5\sigma$ , we can be confident that it is due to new physics.

There are also tensions in the quantities [28]

$$R_{K^{(*)}} = \frac{\Gamma(B \rightarrow K^{(*)}\mu^+\mu^-)}{\Gamma(B \rightarrow K^{(*)}e^+e^-)}. \quad (2.38)$$

LHCb measured  $R_K$  between 1 and 6 GeV, and found a disagreement with the SM value [29,30] of  $2.6\sigma$  [31]. LHCb also measured  $R_{K^*}$  in 2 bins ( $0.045 < q^2 < 1.1 \text{ GeV}^2$  and  $1.1 < q^2 < 1.6 \text{ GeV}^2$ ), and reported disagreement with the SM prediction [32–39] of  $2.1\text{--}2.3\sigma$  and  $2.4\text{--}2.5\sigma$  respectively [40].

Each of these anomalies points to one potential new physics scenario: lepton flavour violation (LFV), a breakdown of the lepton flavour universality in the SM discussed in Sec. 2.2. A consequence of LFV would be that the different leptons generations would no longer have the same coupling to gauge fields. For example, imagine couplings like  $U_{ij}\bar{e}_L^i W^+ \nu_L^j$ , where  $U_{ij}$  is unitary but non-diagonal, then the different lepton generations would have different couplings to  $W$ . This can lead to a

modification of the  $B \rightarrow D^{(*)}l\nu$  and  $B \rightarrow K^{(*)}\bar{l}l$  decays rates by different amounts depending on the lepton flavours in the final state, resulting in the ratios  $R_{D^{(*)}}$ ,  $R_{K^{(*)}}$  deviating from the SM prediction.

There are broadly speaking two ways one can explain LFV. The first is to posit that there are in fact right-handed neutrinos,  $\nu_R$ , and neutrinos have Dirac mass terms  $m\bar{\nu}_L\nu_R$ , from their coupling with the Higgs, just like the charged leptons and quarks. Then, the argument preventing the presence of non-trivial lepton flavour structure in  $\mathcal{L}_{\text{FCCC}}$  breaks down, we obtain an equivalent of the CKM matrix for leptons (the Pontecorvo-Maki-Nakagawa-Sakata (PMNS) matrix), and lepton flavour violation is mediated by the  $W$ . Neutrinos have in fact already been shown to have mass, the PMNS matrix exists, and its elements have been measured. However, as mentioned already, these effects would be extremely small due to the extreme lightness of the neutrinos. Experiments have looked for evidence of  $W$ -mediated LFV processes,  $\tau \rightarrow \mu\gamma$  and  $\mu \rightarrow e\gamma$ , and they found upper bounds for their branching fractions of  $4.2 \times 10^{-13}$  [41] and  $3.1 \times 10^{-7}$  [42] respectively.

Besides there being no evidence for  $W$ -mediated LFV, this picture of neutrino masses is not very aesthetically satisfying. It requires unnaturally small Yukawa couplings between the Higgs and the neutrinos. The second, and much more popular approach, to explaining both LFV and neutrino masses, is the presence of new physics.

In the face of evidence against the SM, the most general way to parameterise the space of possible new physics models is to study the Standard Model Effective Theory (SMEFT). In this approach, one introduces a higher dimension, non-renormalisable operators to the standard model (the SM has only renormalisable dimension 4 operators), and impose a hard momentum cutoff  $\Lambda$ . Then, the SMEFT is

$$\mathcal{L}_{\text{SMEFT}} = \mathcal{L}_{\text{SM}} + \sum_i \frac{c_i^{(5)}}{\Lambda} \mathcal{O}_i^{(5)} + \sum_i \frac{c_i^{(6)}}{\Lambda^2} \mathcal{O}_i^{(6)} + \dots \quad (2.39)$$

where  $\mathcal{O}_i^{(d)}$  is the set of dimension- $d$  operators that satisfy the symmetries of the SM, and  $c_i^{(d)}$  are coefficients to be measured, known as Wilson coefficients. Wilson coefficients differing from the SM expectation can be evidence that the SM must be augmented with new fields at energies above  $\Lambda$ , and the quantum numbers of the associated operators gives information about the quantum numbers of the new fields.

One can fit the available  $B \rightarrow D^{(*)}l\bar{\nu}$  and  $B \rightarrow K^{(*)}\bar{l}l$  data to predictions from

SMEFT, in order to infer the Wilson coefficients necessary to explain the anomalies. In [43] it was found that  $R_{D(*)}$  can be explained with the  $d = 6$  operators

$$\begin{aligned} (\bar{c}\gamma_\mu P_L b)(\bar{\tau}\gamma^\mu P_L \nu_\tau), \quad (\bar{c}\sigma^{\mu\nu} P_L b)(\bar{\tau}\sigma_{\mu\nu} P_L \nu_\tau), \quad (\bar{\tau}P_L c^c)(\bar{b}^c P_L \nu_\tau), \\ (\bar{\tau}\gamma_\mu P_R b)(\bar{c}\gamma^\mu P_L \nu_\tau), \quad (\bar{\tau}\gamma_\mu P_L b)(\bar{c}\gamma^\mu P_L \nu_\tau), \quad (\bar{\tau}P_R c^c)(\bar{b}^c \gamma^\mu P_L \nu), \end{aligned} \quad (2.40)$$

where  $P_{L/R} = (1 \pm \gamma_5)/2$ ,  $\psi^c = -i(\bar{\psi}\gamma^0\gamma^2)^T$  and  $\bar{\psi}^c = -i(\gamma^0\gamma^2\psi)^T$ . In [28], a similar process found the operators necessary to explain  $R_{K(*)}$ :

$$\begin{aligned} (\bar{s}\gamma_\mu P_L b)(\bar{e}\gamma^\mu e), \quad (\bar{s}\gamma_\mu P_L b)(\bar{\mu}\gamma^\mu \mu) \\ (\bar{s}\gamma_\mu P_L b)(\bar{e}\gamma^\mu \gamma_5 e), \quad (\bar{s}\gamma_\mu P_L b)(\bar{\mu}\gamma^\mu \gamma_5 \mu) \end{aligned} \quad (2.41)$$

This information, along with constraints from other measurements, strongly reduces the space of possible new physics models that could produce these anomalies. Hot topics include Leptoquarks,  $Z'$  models, and partial compositeness [28, 43–45].

## 2.3 Strong Interaction Physics

The work of this thesis is essentially quantifying the effect the strong interaction has on branching fractions for semileptonic decays. The strong interaction and the observed pattern of hadrons can be explained with Quantum Chromodynamics (QCD). In this section we review the fundamental theory, and the force's physical features.

### 2.3.1 Quantum Chromodynamics

QCD is an  $SU(3)$  Yang-Mills gauge theory. The Lagrangian is derived by requiring:

- $N_f$  fermion fields transforming in the fundamental representation of the  $SU(3)_C$  gauge group.
- Invariance under that gauge group.
- Renormalizability of all interactions.

From these we find [46]

$$\mathcal{L}_{\text{QCD}} = \sum_i \bar{q}_i (iD^\mu - m_i) q_i - \frac{1}{4} \text{Tr} G_{\mu\nu} G^{\mu\nu} - g \frac{\bar{\theta}}{64\pi^2} \epsilon^{\mu\nu\rho\sigma} \text{Tr} G_{\mu\nu} G_{\rho\sigma} \quad (2.42)$$

$$D_\mu = \partial_\mu - igG_\mu, \quad G_{\mu\nu} = [D_\mu, D_\nu].$$

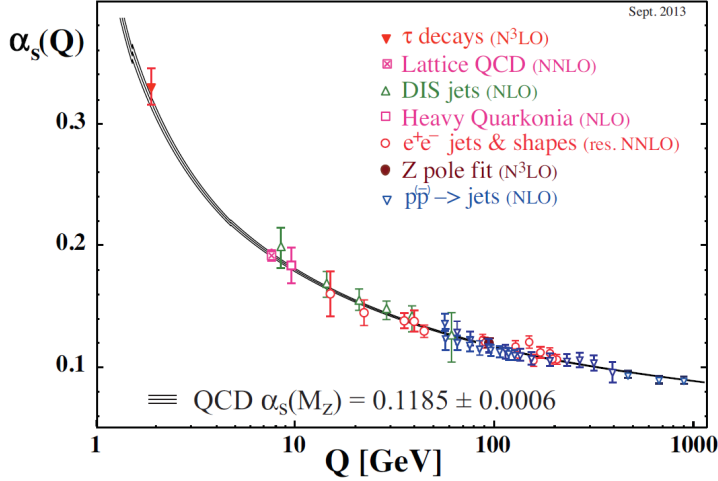


Figure 2.8: The relationship between scale  $Q$  and the strong coupling constant  $\alpha_s$ , from the PDG [1].

$q_i = (q_{i,r}, q_{i,b}, q_{i,g})$  are the  $N_f$  fermions, vectors in *color space*, transforming under

$$q_i(x) \rightarrow \Lambda(x)q_i(x), \quad \bar{q}_i(x) \rightarrow \bar{q}_i(x)\Lambda^\dagger(x), \quad (2.43)$$

where  $\Lambda(x)$  is an  $SU(3)$  matrix acting on color the color space.  $G_\mu$  are the  $\mathfrak{su}(3)$ -valued gluon fields, transforming under the Gauge group like

$$G_\mu(x) \rightarrow \Lambda(x)G_\mu(x)\Lambda^\dagger(x) - \frac{i}{g}[\partial_\mu\Lambda(x)]\Lambda^\dagger(x). \quad (2.44)$$

$g$  is the coupling constant of the theory, often expressed instead as  $\alpha_s = (g/4\pi)^2$ .  $\bar{\theta}$  has strong experimental bounds on it's size, to the extent that for our purposes it can be neglected [47].

The most notable feature of QCD is due to the running of the QCD coupling  $\alpha_s$  [48]. In contrast with the electroweak force, the coupling of the strong force diverges at low energies. This is referred to as *asymptotic freedom*. At energies around or below  $\Lambda_{\text{QCD}} \sim 0.5\text{GeV}$ ,  $\alpha_s$  becomes too large to be a good expansion parameter, and perturbation theory becomes unreliable for making predictions.

At large  $\alpha_s$ , quarks and gluons become strongly interacting, this is believed to be the source of confinement, the mechanism that bounds quarks together into hadrons.

Broadly speaking there are two approaches to QCD at low energies:

1. Chiral Perturbation theory - an effective theory of hadrons with the same symmetry properties as QCD.

2. Lattice simulations - solve the path integral by brute force, eliminating the need for an expansion in  $\alpha_s$ . This is covered in chapters 3 and 4, since it is the method used in the work presented in this thesis.

### 2.3.2 Chiral Symmetry

In the limit of  $m_i \rightarrow 0 \forall i$ , QCD develops two new global symmetries between the flavours;

$$q_i \rightarrow \exp(i\theta_a \lambda_a^{ij}) q_j \quad (2.45)$$

$$q_i \rightarrow \exp(i\gamma_5 \theta_a \lambda_a^{ij}) q_j \quad (2.46)$$

where  $\lambda_a$  are  $U(N_f)$  matrices. They are labelled  $U(N_f)_V$  and  $U(N_f)_A$  respectively, standing for vector and axial-vector.

Via Noether's theorem, these symmetries imply currents that are conserved in the massless limit [49];

$$V_\mu^a = \bar{q} \gamma_\mu \lambda_a q \quad , \quad A_\mu^a = \bar{q} \gamma_\mu \gamma_5 \lambda_a q \quad (2.47)$$

The way in which the chiral symmetry is realised in quantum mechanics is captured by the *Ward identities*. There is an infinite number of possible Ward identities, but for the purpose of our work, we only need to consider the most simple of them.

Consider the partition function for QCD:

$$\mathcal{Z} = \int [d\psi d\bar{\psi} dA] e^{iS[\psi, \bar{\psi}, A]}, \quad (2.48)$$

where  $[d\psi d\bar{\psi} dA]$  represents the functional integral over quark, antiquark and gauge fields. Consider performing a shift of the integration variables of the form (2.45), and allow the parameters  $\theta_a$  to be local,  $\theta_a = \theta_a(x)$ . The partition function becomes

$$\mathcal{Z} = \int \mathcal{J}[d\psi d\bar{\psi} dA] (1 + i\delta S) e^{iS[\psi, \bar{\psi}, A]} \quad (2.49)$$

$\mathcal{J}$  is the Jacobian of the measure  $[d\psi d\bar{\psi} dA]$  under the coordinate transform (2.45). In many cases,  $\mathcal{J}$  will be non-trivial, due to either regularization schemes that don't respect the symmetry or quantum anomalies. The symmetries we are concerned with here are anomaly free, so  $\mathcal{J} = 1$ .

The effect of the local version of (2.45) on the action is

$$\delta S = \int d^4x \theta_a(x) [\partial_\mu V_a^\mu(x) - i\bar{q}(x)[\lambda_a, M]q(x)], \quad (2.50)$$

where  $M = \text{diag}(m_u, m_d, m_s, \dots)$  acts on flavour. Setting the arbitrary parameters  $\theta_a(x)$  to 1 and removing  $\mathcal{Z}$  from each side of (2.49), and removing the spacetime integral  $\int d^4x$  results in

$$\partial_\mu \langle V_a^\mu \rangle = i \langle \bar{q}[\lambda_a, M]q \rangle, \quad (2.51)$$

where  $\langle \rangle$  represents a quantum expectation value, the state the expectation value is taken need not be specified since the above derivation does not assume any particular state. Repeating the above steps with the vector chiral transform replaced with the axial-vector chiral transform, one finds

$$\partial_\mu \langle A_a^\mu \rangle = i \langle \bar{q}\{\lambda_a, M\}q \rangle. \quad (2.52)$$

(2.51) and (2.52) are examples of Ward identities, they describe the non-conservation of the chiral currents.

A useful theorem [50] is that partially conserved currents (currents that become conserved when some parameter in the theory vanishes, like  $V_a^\mu$  and  $A_a^\mu$ ) require no renormalisation under any regularisation scheme. The conserved or partially conserved current  $J_a^\mu$  has a corresponding charge  $Q_a(t) = \int d^3x J^0(\underline{x}, t)$  that is the generator of it's corresponding symmetry transform on Hilbert space. In this case, these charges are members of the Lie algebra of the symmetry group;

$$[Q_a(t), Q_b(t)] = if_{abc}Q_c(t), \quad (2.53)$$

where  $f_{abc}$  are the structure constants of the algebra. Under some regularisation, change in regularisation scheme, or running of scale, each operator in the theory may require multiplicative renormalisations;  $Q_a \rightarrow Z_Q Q_a$ . Equation (2.53) demands that  $Z_Q = 1$ , so  $J^0$  obtains no renormalisation, and if the regularization is lorentz invariant, this carries on to  $J^\mu$ .

Since one can transform any flavour into any other flavour via the chiral  $U(N_f)$  generators, one can build currents charged with any combination of flavours from linear combinations of  $V_a^\mu$  and  $A_a^\mu$ ;

$$V_{ij}^\mu = \bar{q}_i \gamma^\mu q_j, \quad \partial_\mu \langle V_{ij}^\mu \rangle = i(m_i - m_j) \langle S_{ij} \rangle \quad (2.54)$$

$$A_{ij}^\mu = \bar{q}_i \gamma^\mu \gamma^5 q_j, \quad \partial_\mu \langle A_{ij}^\mu \rangle = i(m_i + m_j) \langle P_{ij} \rangle \quad (2.55)$$

where we have defined  $S_{ij} = \bar{q}_i q_j$  and  $P_{ij} = \bar{q}_i \gamma^5 q_j$ , the scalar and pseudoscalar densities. The non-renormalisation of  $V_a^\mu$  and  $A_a^\mu$  carry on to  $V_{ij}^\mu$  and  $A_{ij}^\mu$ , and onto the operators  $(m_i - m_j)S_{ij}$ ,  $(m_i + m_j)P_{ij}$  via the Ward identities.

The partially conserved currents  $V_\mu^{ij}$  and  $A_\mu^{ij}$  are the same currents that feature in the matrix element of leptonic and semileptonic decays in Sec. 2.2, and their expectation values appear in amplitudes for leptonic and semileptonic decays. Hence, the fact that these can be related to alternative expectation values via ward identities, and that they obtain no renormalisation, is very useful in the calculation of these amplitudes.

## 2.4 Heavy Quark Physics

Quarks with mass  $m_Q \gg \Lambda_{\text{QCD}}$  are referred to as heavy quarks. Charm and bottom quarks are considered heavy:  $\Lambda_{\text{QCD}}/m_c \sim 1/4$ ,  $\Lambda_{\text{QCD}}/m_b \sim 1/14$ . This separation of scales can come in very useful. They mean one can integrate out the degrees of freedom at  $m_Q$ , and still have a good description of the dynamics at  $\Lambda_{\text{QCD}}$ . This philosophy gives rise to Heavy Quark Effective Theory (HQET). We will summarise the aspects of this theory most relevant to our work.

### 2.4.1 HQET

HQET is an effective field theory with the cutoff at the heavy quark mass  $m_Q$ , and terms organized in a series in  $\Lambda_{\text{QCD}}/m_Q$ . Since at the  $b$  (and  $c$ ) mass QCD is perturbative ( $\alpha_s(m_Q) \ll 1$ ), one can match HQET to perturbative QCD at  $m_Q$ , then run the couplings of HQET down to produce useful predictions at the confinement scale.

#### HQET Lagrangian

We will derive HQET for a single heavy quark interacting with gluons, the generalization to many flavours is straightforward. The fermion part of the Lagrangian is

$$\mathcal{L}_{\text{QCD}} = \bar{Q}(iD - m_Q)Q, \quad (2.56)$$

where  $Q$  is the heavy quark field. Define the heavy quark velocity  $v$  according to  $v = p_Q/m_Q$ . Split  $Q$  into ‘‘heavy’’ and ‘‘light’’ components:

$$Q = h + H \quad : \quad h = \frac{1}{2}e^{-im_Q v \cdot x}(1 + \not{v})Q \quad (2.57)$$

$$H = \frac{1}{2}e^{-im_Q v \cdot x}(1 - \not{v})Q \quad (2.58)$$

with the important property

$$\not{p}h = h \quad \not{p}H = -H. \quad (2.59)$$

In terms of these new fields the Lagrangian becomes

$$\mathcal{L}_{\text{QCD}} = i\bar{h}(v \cdot D)h - \bar{H}(i(v \cdot D) - 2m_Q)H + i\bar{h}\not{D}^\perp H + i\bar{H}\not{D}^\perp h. \quad (2.60)$$

where  $v_\mu(v \cdot D)$  is the covariant derivative projected along the direction of  $v$ , and  $D^\perp = D - v_\mu(v \cdot D)$  are the components perpendicular to  $v$ . A physical interpretation of the definition of  $h$  in (2.57) can be seen by acting a spacial derivative on the definition of  $h$ , and by recognising  $\partial Q = -ip_Q$ ,  $\partial h = -ip_h$ , we find that

$$p_Q = m_Q v + p_h. \quad (2.61)$$

Since  $p_h \ll p_Q$ , we see that the quark's momentum is dominated by it's mass (the quark is close to on-shell), and the  $h$  field represents perturbations around on-shell due to interactions with the lighter degrees of freedom at  $\Lambda_{\text{QCD}}$ .

From (2.60), we see that  $h$  is a massless field and  $H$  has a mass of  $2m_Q$ . From this Lagrangian we can derive an equation of motion for  $H$ :

$$(i(v \cdot D) + 2m_Q)H = i\not{D}^\perp h, \quad (2.62)$$

with the solution

$$H = \frac{1}{i(v \cdot D) + 2m_Q}i\not{D}^\perp h = \frac{1}{2m_Q} \sum_{n=0}^{\infty} \frac{(-i(v \cdot D))^n}{2m_Q} \not{D}^\perp h. \quad (2.63)$$

By substituting this into the Lagrangian we arrive at

$$\mathcal{L}_{\text{HQET}} = i\bar{h}(v \cdot D)h - \bar{h}\not{D}^\perp \frac{1}{2m_Q} \sum_{n=0}^{\infty} \frac{(-i(v \cdot D))^n}{2m_Q} \not{D}^\perp h. \quad (2.64)$$

Since we expect  $v \cdot D \sim \Lambda_{\text{QCD}}$ , we can interpret the infinite sum as a series in  $\Lambda_{\text{QCD}}/m_Q$ , and truncate it at some order.

Leading order HQET exhibits new symmetries not present in full QCD, known as the heavy quark symmetries. Since  $m_Q$  is not present in the leading order Lagrangian, there is a flavour symmetry - a set of  $N$  heavy quarks with the same  $v$  can be mixed via an  $SU(N)$  symmetry. Similarly, due to the absence of spin-mixing matrices, a heavy quark has an  $SU(2)$  spin symmetry. This builds up a physical picture of a heavy quark in a meson being a static colour charge, the dynamics at  $\Lambda_{\text{QCD}}$  are not effected by its mass or spin.

We will now use HQET to derive a useful theorem used in our work.

### Luke's Theorem

Luke's theorem, which can be derived from the Ademollo-Gatto (AG) theorem, tells us the leading order heavy quark mass dependence of form factors. First we will derive the AG theorem. We will follow the proof given in [51].

Consider the transition amplitude

$$\langle \alpha | Q_a | \beta \rangle, \quad (2.65)$$

where  $Q_a$  is a conserved charge associated with some global symmetry  $\mathcal{G}$ , and  $|\alpha\rangle$  and  $|\beta\rangle$  belong to an irrep of  $\mathcal{G}$ . Imagine explicitly breaking the symmetry with a term like  $\mathcal{L}_{\text{break}} = \lambda \mathcal{O}_{\text{break}}$ . The states in the broken theory can be expressed as

$$|\beta\rangle = c_{\beta\beta} |\beta'\rangle + \sum_m c_{\beta m} |m'\rangle \quad (2.66)$$

$$\langle \alpha | = c_{\alpha\alpha}^* \langle \alpha' | + \sum_n c_{\alpha n}^* \langle n' |. \quad (2.67)$$

where primed states are the new basis of states belonging to irreps of  $\mathcal{G}$ , after the breaking. Here  $|m'\rangle$  can only be states that can be mixed with  $|\beta\rangle$  by  $\mathcal{O}_{\text{break}}$ , i.e., via the broken dynamics of the theory. Similarly for  $\langle n' |$  and  $\langle \alpha |$ . The transition amplitude becomes

$$\begin{aligned} \langle \alpha | Q_a | \beta \rangle &= c_{\alpha\alpha}^* c_{\beta\beta} \langle \alpha' | Q_a | \beta' \rangle \\ &+ \sum_m c_{\alpha\alpha}^* c_{\beta m} \langle \alpha' | Q_a | m' \rangle \\ &+ \sum_n c_{\alpha n}^* c_{\beta\beta} \langle n' | Q_a | \beta \rangle \\ &+ \sum_m \sum_n c_{\alpha n}^* c_{\beta m} \langle n' | Q_a | m' \rangle. \end{aligned} \quad (2.68)$$

The theorem applies to the situation where  $|n'\rangle$  and  $|m'\rangle$  live in different  $\mathcal{G}$  irreps to  $|\alpha\rangle$  and  $|\beta\rangle$  (we assume  $|\alpha\rangle$  and  $|\beta\rangle$  to be in the same irrep otherwise the transition amplitude would vanish). In this case the amplitudes in the second and third terms vanish. Now consider the order of the coefficients  $c_{nm}$ . We can assume that  $c_{nm} = \mathcal{O}(\lambda)$  for arbitrary  $n, m \neq \alpha, \beta$ , since switching off the symmetry breaking by setting  $\lambda = 0$  should cause  $|\alpha\rangle$  and  $|\alpha'\rangle$  to coincide. Then, using the normalization of the states  $\sum_n |c_{\alpha n}|^2 = 1$ , we find  $c_{\alpha\alpha} = \sqrt{1 - \mathcal{O}(\lambda)^2} = 1 + \mathcal{O}(\lambda^2)$ , and similarly for  $c_{\beta\beta}$ . Applying this to the two surviving terms in (2.68), we end up with

$$\langle \alpha | Q_a | \beta \rangle = 1 + \mathcal{O}(\lambda^2) \quad (2.69)$$

This is the AG theorem: if the current  $Q_a$  and the symmetry breaking term  $\mathcal{O}_{\text{break}}$  act orthogonally on the states, the transition amplitude can have at most a second order correction in the symmetry breaking parameter.

Now we will apply this to HQET to produce Luke's theorem. Consider a transition including two heavy quarks ( $b$  and  $c$ ). Then, the heavy quark symmetry is a spin symmetry for each flavour and a flavour symmetry between them. The leading order spin symmetry breaking terms can be found from (2.64) to be

$$\frac{1}{4m_Q} \bar{h} \gamma^\mu \gamma^\nu F_{\mu\nu} h. \quad (2.70)$$

for both  $h = b$  and  $h = c$ . The leading order flavour breaking term is

$$\left( \frac{1}{2m_b} - \frac{1}{2m_c} \right) \frac{1}{2} \bar{h} \sigma_z \not{D}^{\perp 2} h, \quad (2.71)$$

where now  $h = (b, c)$  and the  $\sigma_z$  is the third pauli matrix acting on flavour. These terms cause states, for example  $|B\rangle$  to mix with states  $|n'\rangle$ , each being of the order of at least one of the following:  $1/2m_b, 1/2m_c$ , and  $(1/2m_b - 1/2m_c)$ . It can be shown [51] that the leading order symmetry breaking terms can only mix pseudoscalar and vector mesons with other irreps of the heavy quark symmetries. Hence, for example, in the  $B \rightarrow D^*$  transition we can write

$$\langle D | \bar{c} \gamma_\mu b | B \rangle = \xi + \mathcal{O} \left( \left( \frac{1}{2m_b} - \frac{1}{2m_c} \right)^2 \right), \quad (2.72)$$

$$\langle D | \bar{c} \gamma_\mu \gamma_5 b | B \rangle = \xi + \mathcal{O} \left( \left( \frac{1}{2m_b} - \frac{1}{2m_c} \right)^2 \right). \quad (2.73)$$

where  $\xi$  is some  $b$ - and  $c$ -mass independent number.

This carries onto the pseudoscalar-vector and pseudoscalar-pseudoscalar form factors at zero recoil

$$h_{A_1}(1) = \eta_A \left( 1 + \frac{l_V}{(2m_c)^2} + \frac{l_A}{m_b m_c} - \frac{l_P}{(2m_b)^2} \right), \quad (2.74)$$

$$h_+(1) = \eta_V \left( 1 - l_P \left( \frac{1}{(2m_b)^2} - \frac{1}{(2m_c)^2} \right) \right), \quad (2.75)$$

where here  $h_+$  comes from an HQET-inspired parameterisation of pseudoscalar-pseudoscalar transition amplitudes alternative to (2.28):

$$\frac{\langle M' | V_\mu^{q_1 q^2} | M \rangle}{\sqrt{Mm}} = h_+(w)(v + v')_\mu + h_-(w)(v - v')_\mu. \quad (2.76)$$

The factors  $\eta_{A,V}$  in (2.74) and (2.75) are matching factors between QCD and HQET, and can contain logarithms of heavy masses. The factors  $l_{V,A,P}$  are free non-perturbative parameters that must be fixed by some non-perturbative calculation e.g. a lattice QCD calculation.

### 2.4.2 NRQCD

An effective field theory closely related to HQET is Non-Relativistic QCD (NRQCD). This differs from HQET only by the power counting; instead of organizing terms in the Lagrangian according to their order in  $\Lambda_{\text{QCD}}/m$ , the terms are organized in terms of powers of the heavy quark's spacial velocity  $v \sim |\mathbf{p}|/m$ . NRQCD is derived with the following process:

- Separate the quark and antiquark components of the heavy quark. Since a non-relativistic fermion is decoupled from its antiparticle, our action only requires to describe the top two components of a Dirac spinor. Define the antiquark-free 2-component spinor  $h$  via the Foldy-Wouthuysen transformation  $\psi \rightarrow h = e^{\gamma \cdot \mathbf{D}/2m} \psi$  [52]. This acts to remove the  $\gamma \cdot \mathbf{D}$  term from the Dirac part of the Lagrangian, which is the only part that couples the fermion to the anti-fermion.
- Define power-counting by considering the expected expectation values of operators for heavy mesons [53]. The three relevant scales concerning the heavy meson are  $M, p \sim Mv$  and  $E_K \sim Mv^2$ , where  $M$  is the meson mass,  $p$  the spacial momentum and  $E_K$  the kinetic energy. By relating operators to these three scales, we deduce their order in  $v$ . Start with the normalization of a scalar current:

$$\langle M | \int d^3x h^\dagger(x) h(x) | M \rangle \sim 1, \quad (2.77)$$

where  $|M\rangle$  is some heavy meson state. Since we expect the meson state to be localized in a region of size  $1/p$ , we can assert that

$$\int d^3x \sim \frac{1}{p^3}. \quad (2.78)$$

From this and (2.77), we find  $h \sim p^{3/2} \sim v^{3/2}$ . The order of the derivative operator can be deduced from

$$E_K = \langle M | \int d^3x h^\dagger(x) \frac{D^2}{2M} h(x) | M \rangle \quad (2.79)$$

to be  $D \sim v$ . Following such a chain of arguments, we can deduce the order in  $v$  of any operator.

- The Lagrangian to  $\mathcal{O}(v^n)$  is then simply all of the operators satisfying the symmetries of QCD of orders below  $v^n$ , with some Wilson coefficients [53]. To  $\mathcal{O}(v^6)$ :

$$\begin{aligned} \mathcal{L}_{\text{NRQCD}} = & h^\dagger \left( iD_0 + \frac{\mathbf{D}^2}{2m} + c_1 \frac{\mathbf{D}^4}{m^3} + c_2 g \frac{\mathbf{D} \cdot \mathbf{E} - \mathbf{E} \cdot \mathbf{D}}{m^2} \right. \\ & + c_3 ig \frac{\sigma \cdot (\mathbf{D} \times \mathbf{E} - \mathbf{E} \times \mathbf{D})}{m^2} + c_4 g \frac{\sigma \cdot \mathbf{B}}{m} \\ & + f_1 g \frac{\{\mathbf{D}^2, \sigma \cdot \mathbf{B}\}}{m^3} + f_2 ig \frac{\{\mathbf{D}^2, \sigma \cdot (\mathbf{D} \times \mathbf{E} - \mathbf{E} \times \mathbf{D})\}}{m^4} + f_3 ig^2 \frac{\sigma \cdot \mathbf{E} \times \mathbf{E}}{m^3} \Big) h \\ & + d_1 \frac{(h^\dagger H)(H^\dagger h)}{m^2} + d_2 \frac{(h^\dagger \sigma H) \cdot (H^\dagger \sigma h)}{m^2} \\ & + d_3 \sum_a \frac{(h^\dagger T^a H)(H^\dagger T^a h)}{m^2} + d_4 \sum_a \frac{(h^\dagger T^a \sigma H) \cdot (H^\dagger T^a \sigma h)}{m^2} \end{aligned} \quad (2.80)$$

$\mathbf{E}$  and  $\mathbf{B}$  are the chromoelectric and chromomagnetic fields,  $T^a$  are fundamental representation of the  $SU(3)$  color generators, and  $H$  is the antiquark components of the heavy quark.  $c_{1,2,3,4}, f_{1,2,3}, d_{1,2,3,4}$  are Wilson coefficients, that can be fixed by perturbative matching to full QCD at the cutoff (the heavy quark mass, where QCD is perturbative).

## CHAPTER 3

# Lattice Quantum Chromodynamics

---

As discussed in Sec. 2.3.1, at low energies QCD becomes non-perturbative. In other words, the coupling  $\alpha_s$  becomes  $\mathcal{O}(1)$ , and an expansion in  $\alpha_s$  (as in perturbation theory) will not be dominated by the leading orders. In order to calculate observables of low energy QCD (like hadronic form factors), we require an alternative to perturbation theory.

The expectation value of an observable  $\mathcal{O}$  in a Yang-Mills theory can be expressed as a path integral;

$$\langle \mathcal{O} \rangle = \frac{1}{Z} \int [dG d\psi d\bar{\psi}] \mathcal{O} e^{iS[G, \psi, \bar{\psi}]}, \quad (3.1)$$

where  $G$  is the gauge field,  $\psi(\bar{\psi})$  are the (anti)fermion fields,  $S$  is the classical action, and  $[dG d\psi d\bar{\psi}]$  denotes integration over all configurations of the gauge and fermion fields.  $Z$  is the partition function. In the perturbative approach, we would expand  $\exp(-\text{interacting part of } S)$  resulting in a power series in the gauge coupling populated by Feynman diagrams.

We must instead carry out the integral directly, by numerical brute force. Since it is not numerically feasible to carry out an infinite number of integrals, one must approximate spacetime as a discrete 4-dimensional lattice with spacing “ $a$ ” between lattice sites, finite spacial volume  $L_x^3$  and finite temporal extent  $L_t$ . The functional integral becomes

$$\int [dG d\psi d\bar{\psi}] = \prod_n \int dU(x_n) d\psi(x_n) d\bar{\psi}(x_n), \quad (3.2)$$

where  $n$  is a 4-vector with integer components labelling the sites, and  $x_n^\mu = an^\mu$ . This has a second benefit which is to naturally regularize the theory with a momentum cutoff  $\Lambda \sim 1/a$ . The gauge field has been replaced with the *gauge link*  $U$ , to be defined in the following section.

We require the lattice also to be finite in size, in this thesis we use only lattices that have the same number ( $N_x$ ) of sites in each spatial direction. We use lattices that have periodic boundary conditions in the temporal direction, i.e  $\psi(x + aN_t \hat{t}) = \psi(x)$  etc.

To avoid having to integrate over imaginary numbers (equivalently to avoid the scourge of the *sign problem* [54]), one also performs a *Wick rotation*. This is the redefinition  $t \rightarrow it$ , which changes the metric from Minkowski to Euclidean, and changes the weight  $\exp(iS) \rightarrow \exp(-S)$ . This has the advantage that it turns the quantum path integral into simply an average in statistical mechanics, this means we can apply all of the machinery of statistical mechanics to computing expectation values.

To obtain the 'real world' result for some expectation value, where real world means  $a = 0$ , one must perform the path integral at a number of different  $a$  values, and then extrapolate the results to  $a = 0$ .

One must choose a discretized version of the QCD action, one that becomes continuum QCD in the continuum ( $a \rightarrow 0$ ) limit. This is a far from trivial step. There is an infinite number of choices of lattice actions that become QCD in the continuum limit. There therefore is a huge literature of different choices of discrete lattice actions. Different collaborations use different actions, and there is never-ending argument about the merits and pitfalls of each.

The rest of this chapter is dedicated to motivating and detailing the choices of discretisation used in the work of this thesis.

### 3.1 Lattice Gauge Fields

Often the best way to introduce some sophisticated method or technique is to first show how the naive approach breaks down. Imagine attempting a naive discretisation of the QCD action. Derivatives can be replaced with something like

$$\partial_\mu f(x) \rightarrow \frac{1}{2a} (f(x + a\hat{\mu}) - f(x - a\hat{\mu})) \quad (3.3)$$

where  $\hat{\mu}$  is the unit vector in the  $\mu$  direction. The quark kinetic part of the QCD action,  $\bar{q}\not{D}q$ , becomes

$$\frac{1}{2a} \bar{q}(x)\gamma^\mu q(x + a\hat{\mu}) - \frac{1}{2a} \bar{q}(x)\gamma^\mu q(x - a\hat{\mu}) - ig\bar{q}(x)G_\mu(x)\gamma^\mu q(x). \quad (3.4)$$

This is no longer invariant under the gauge trasforms (2.43), for example the first term becomes  $\bar{q}(x)\Lambda(x)^\dagger\Lambda(x+a\hat{\mu})q(x+a\hat{\mu})$ . The finite distance between lattice sites

force us to think more carefully about the interpretation of gauge symmetry on a lattice.

Formally speaking, a gauge field is a connection on a fibre bundle. So what does that all mean?

At each point  $x$ , there is a space of possible vectors that a quark field  $q(x)$  could be, call it  $V_x$ . In this case, this is the colour space, the space of colour vectors (this refers to a single flavour, we suppress the flavour index here for brevity).  $V_x$  is a *fibre*. Spacetime, in our case  $\mathbb{E}^4$ , is called the *base space* in this context.

The problem with our non-gauge-invariant terms above is that we are trying to compare vectors in different fibres. To compare colour vectors at two different spacetime points, i.e. two different fibres, one must *parallel transport* the vector from one point to another, according to some rule of how it changes, the so-called *connection*. In our case the parallel transport is a Wilson line:

$$\begin{aligned} W(x, y) : V_y &\rightarrow V_x, \\ W(x, y) &= Pe^{ig \int dc \cdot G}. \end{aligned} \quad (3.5)$$

where  $c$  is some curve between  $x$  and  $y$ , and  $P$  orders the operation of the gauge field  $G$  on the fibres, i.e. it operates at  $x$  first and  $y$  last. A wilson line transforms under the gauge group like  $W(x, y) \rightarrow \Lambda(x)W(x, y)\Lambda^\dagger(y)$ , so operators like  $\bar{q}(x)W(x, y)q(y)$  are gauge-invariant, reflecting the fact that the color vector  $q(y)$  has been parallel transported into the same fibre as  $\bar{q}(x)$ .

From this we see that, on a lattice, the natural degrees of freedom are no longer the elements of the Lie algebra,  $G_\mu$ , but Wilson lines connecting adjacent lattice sites, also known as *links*:

$$U_\mu(x) \in SU(N_c) : V_x \rightarrow V_{x+a\hat{\mu}}, \quad (3.6)$$

that Gauge transform like

$$U_\mu(x) \rightarrow \Lambda(x)U_\mu(x)\Lambda^\dagger(x + a\hat{\mu}). \quad (3.7)$$

Then, a bilinear of colour vectors at any two points can be made to be gauge invariant by including a path between them made of links. For example;

$$\begin{aligned} \bar{q}(x)U_\mu(x)q(x + a\hat{\mu}) &\rightarrow [\bar{q}(x)\Lambda^\dagger(x)](\Lambda(x)U_\mu(x)\Lambda^\dagger(x + a\hat{\mu}))[\Lambda(x + a\hat{\mu})q(x + a\hat{\mu})] \\ &= \bar{q}(x)U_\mu(x)q(x + a\hat{\mu}). \end{aligned} \quad (3.8)$$

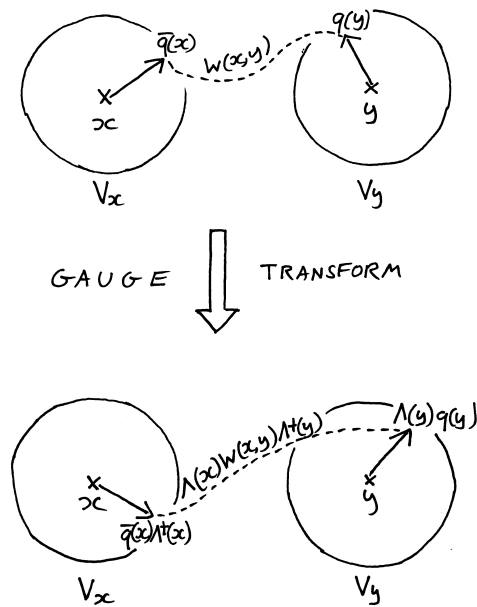


Figure 3.1: Depiction of colour spaces (fibres) at two points in spactime (base space) with the value of the quark field  $q$  represented at each point as a colour vector, and the connection  $W(x,y)$  needed to compare the two colour vectors. A gauge transform changes the two vectors in different ways, for the comparison to be gauge independent, the connection must also transform appropriately.

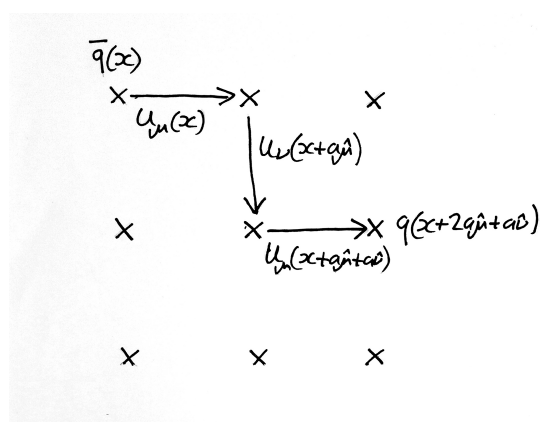


Figure 3.2: Depiction of a gauge invariant quark bilinear, connected by a Wilson line made of gauge links.

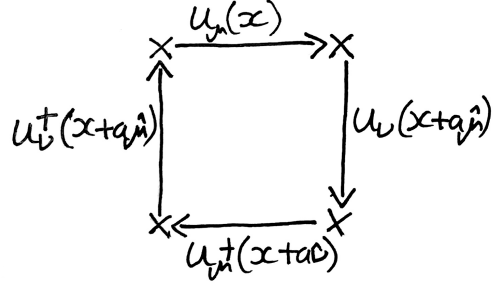


Figure 3.3: Elementary Plaquette.

The  $\bar{q}Dq$  term in the QCD Lagrangian can then be represented on the lattice in a Gauge invariant way by

$$\frac{1}{2a} \bar{q}(x) \gamma_\mu (U_\mu(x) q(x + a\hat{\mu}) + U_\mu^\dagger(x - a\hat{\mu}) q(x - a\hat{\mu})). \quad (3.9)$$

If one defines the links in terms of the continuum gauge fields  $G_\mu$  via

$$U_\mu(x) = \exp \left( ig a G_\mu \left( x + \frac{a\hat{\mu}}{2} \right) \right), \quad (3.10)$$

then (3.9) takes the correct form in the continuum limit, i.e. it becomes  $\bar{q}Dq + \mathcal{O}(a^2)$ .

### 3.1.1 The Gauge Action

We must design a pure gauge part of the action in terms of link variables. It is clear that the only gauge-invariant operator that depends only on the link variables are closed loops of links, as in fig. 3.3.

This brings us basically all the way to the correct answer. The simplest lattice discretisation of the Yang-Mills action is the real part of the smallest possible closed loop of gauge links;

$$S_G = -\frac{1}{g^2} \sum_x \sum_{\mu \neq \nu} \text{Re} \text{Tr}(1 - \square_{\mu\nu}(x)), \quad (3.11)$$

$$\square_{\mu\nu} = U_\mu(x) U_\nu(x + a\hat{\mu}) U_\mu^\dagger(x + a\hat{\nu}) U_\nu^\dagger(x). \quad (3.12)$$

$\square_{\mu\nu}$  is called the *elementary plaquette*. In the continuum limit this action reduces to

$$S_G = \frac{1}{4} \int d^4x \text{Tr} G_{\mu\nu} G^{\mu\nu} + \mathcal{O}(a^2), \quad (3.13)$$

as required.

This lattice action has a sensible interpretation in terms of the geometrical interpretation of gauge theory. The gauge force is due to *curvature* in the gauge field, a path-dependence in parallel transport. The gauge force is due to the presence of curvature, and the simplest local measure of the curvature is the plaquette.

In fact, any closed loop reduces to the Yang-Mills action in the continuum. This can be seen intuitively, taking the continuum limit means shrinking any closed loop into an infinitesimally small point. We then have a choice of gauge action on the lattice.

### 3.1.2 Symmanzik Improvements of the Gauge Action

Any lattice action is admissible for a calculation as long as it reduces to the appropriate QCD action in the continuum. This gives us a lot of freedom in how we chose our lattice action.

This freedom can be exploited in order to push expectation values of observables on the lattice closer to their continuum values (reduce the 'discretisation effects').

This program is known as *Symmanzik improvement*.

In general, a sensible lattice action looks like

$$S = \sum_i c_i(g) \mathcal{O}_{\text{lat}}^i = z_0(\{c_i\}) S_{\text{cont}} + a^2 \sum_{n=1} z_n(\{c_i\}) S_n \quad (3.14)$$

where  $S_{\text{cont}}$  is the continuum action. We are free to choose any  $\{c_i\}$  such that  $z_0(\{c_i\}) = 1$ . In every example we are concerned with,  $\mathcal{O}(a)$  terms are absent, but the argument carries straightforwardly to situations with  $\mathcal{O}(a)$  corrections. A fundamental postulate of the Symmanzik approach is that improvement (removal of discretisation effects) of one observable results in improvement of all other observables. With this in mind, a reasonable approach is:

- Choose some set of lattice operators  $\{\mathcal{O}_{\text{lat}}^i\}$ . The number of operators required can be deduced by looking at the number of allowed irrelevant operators in the continuum theory at the mass dimension of the order of  $a$  you want to remove, i.e. the number of  $S_n$  operators in (3.14).
- Inspect the continuum limit of lattice action to find  $z_0(\{c_i\})$ , enforce  $z_0(\{c_i\}) = 1$ .
- Choose some observable  $\mathcal{O}$  that can be calculated in both the lattice and continuum theory. Use the remaining freedom in  $\{c_i\}$  to remove the leading  $a$

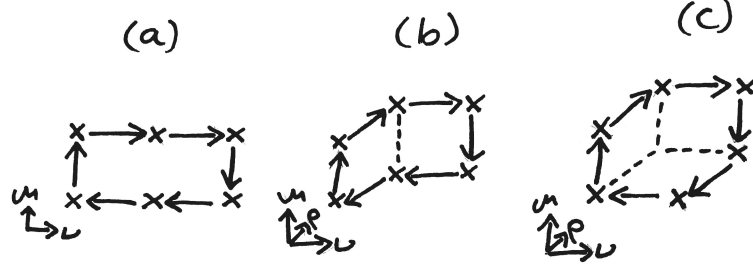


Figure 3.4: Terms additional to the elementary plaquette in the improved pure QCD action.

dependence in  $\langle \mathcal{O} \rangle$  order by order in perturbation theory. i.e., if we write the expectation value as

$$\langle \mathcal{O} \rangle = \sum_{n,m} a^{2n} g^{2m} \langle \mathcal{O}_{n,m}(\{c_i\}) \rangle, \quad (3.15)$$

then this amounts to demanding that  $\langle \mathcal{O}_{1,m}(\{c_i\}) \rangle = 0$ , for as many  $m$ 's as possible.

Applying this to pure QCD, this procedure results in the Lüscher-Weitz action [55]. First consider the number of operators required. In continuum pure QCD, the only dimension 4 operator is  $\text{Tr}G_{\mu\nu}G^{\mu\nu}$ . There are no dimension 5 operators, hence there can be no  $\mathcal{O}(a)$  contribution to the continuum limit of a lattice action. There are three independent dimension 6 operators:

$$\begin{aligned} & \text{Tr}J_{\mu\nu\rho}J_{\mu\nu\rho}, \quad \text{Tr}J_{\mu\mu\rho}J_{\nu\nu\rho}, \quad \text{Tr}J_{\mu\mu\nu}J_{\mu\mu\nu}, \\ & J_{\mu\nu\rho} = [D_\mu, G_{\nu\rho}] \end{aligned} \quad (3.16)$$

Hence we require 3 extra operators in the lattice action to be tuned in order to remove the three contributions from the  $a^2$  terms in (3.14). The simplest choice is to take the plaquette action (3.12), and add all possible Wilson loops containing 6 links. This set consists of three families related by hypercubic invariance, *rectangles* (a), *parallelograms* (b) and *chairs* (c), depicted in fig. 3.4.

So the new lattice action is

$$S_G = -\frac{1}{g^2} \sum_x \sum_{\mu \neq \nu} (-c_0 \text{Re} \text{Tr}(1 - \square_{\mu\nu}(x)) + c_1 \text{Re} \text{Tr}(1 - \square_{\mu\nu}^a(x))) \quad (3.17)$$

$$+ \sum_{\rho \neq \mu, \nu} (c_2 \text{Re} \text{Tr}(1 - \square_{\mu\nu\rho}^b(x)) + c_3 \text{Re} \text{Tr}(1 - \square_{\mu\nu\rho}^c(x))) \quad (3.18)$$

where  $\square_{\mu\nu(\rho)}^{a,b,c}$  are the Wilson loops in fig. 3.4. Expanding this in small  $a$ , one finds the function  $z_0(\{c_i\})$ , setting this to one we find the condition [56];

$$c_0 + 8(c_1 + c_2) + 16c_3 = 1. \quad (3.19)$$

The rest of the freedom must be fixed by comparing observables in the lattice and continuum theories. In [57] for example, by matching the gluon propagator between the two theories, one constrains the coefficients further (at tree level)

$$c_1 = -\frac{1}{12} , \quad c_0 - 8c_3 = \frac{5}{3} \quad (3.20)$$

These are classical relations, so will only prevent lattice artifacts up to  $\mathcal{O}(\alpha_s)$ . For better improvement, one must compare observables that are sensitive to loop corrections. A popular choice of observable is the so-called static quark potential  $V(L)$ , this is the potential energy between two static colour charges, as a function of separation  $aL$  between them.

This procedure is effected by the presence of fermions, so it has been performed a number of times to accommodate different fermion discretisations. In this thesis we report results using the Lüscher-Weitz action for gauge fields and HISQ fermions (see sec. 3.2). The coefficients  $\{c_i\}$  were fixed at one-loop in [58] to be

$$c_0 = \frac{5}{3} + (0.237088(46) - 0.1008(34)N_f)\alpha_s + \mathcal{O}(\alpha_s^2) \quad (3.21)$$

$$c_1 = -\frac{1}{12} + (-0.025218(4) + 0.0110(3)N_f)\alpha_s + \mathcal{O}(\alpha_s^2) \quad (3.22)$$

$$c_2 = 0 + (-0.025218(4) + 0.0110(3)N_f)\alpha_s + \mathcal{O}(\alpha_s^2) \quad (3.23)$$

$$c_3 = 0 \quad (3.24)$$

since these have been tuned to remove  $a^2$  effects up to  $\alpha_s$ , lattice artifacts in observables computed using this action will be of size  $\mathcal{O}(a^2\alpha_s^2)$ , so we say this action is  $\mathcal{O}(a^2\alpha_s)$ -improved.

## 3.2 Lattice Fermions

Putting fermions on the lattice supply a much larger host of complications than gauge fields do. There exist a diverse array of approaches to dealing with fermions on the lattice adopted by different collaborations. Different actions are suited to different types of applications, and intense debates have taken place over the years about the theoretical grounding of various actions. The plethora of fermion actions is due mostly to the famous doubling problem, which we will describe below.

In this chapter we will focus only on the fermion actions used in this work; namely the Highly Improved Staggered Quark (HISQ) action, and the Non-Relativistic QCD (NRQCD) action.

Before beginning the discussion of fermion discretisations, we will define some common notation used for gamma matrices in this context. The Euclidian gamma matrices are defined to obey

$$\{\gamma_\mu, \gamma_\nu\} = 2\delta_{\mu\nu}. \quad (3.25)$$

These have the useful property  $\gamma_\mu^2 = 1$ . The full set of spin-mixing matrices can be labelled according to

$$\gamma_n = \prod_\mu (\gamma_\mu)^{n_\mu}, \quad n_\mu = \mathbb{Z}_2. \quad (3.26)$$

There are 16 such matrices representing corners of the hypercube. One can also use a general site vector  $x_\mu$  to label the matrix, then  $\gamma_x = \gamma_n$  where  $n_\mu = x_\mu/a \bmod 2$ . It is straightforward to show that for any  $n$ ;  $\gamma_n^\dagger \gamma_n = 1$ . We also define  $\gamma_{5\mu} = i\gamma_5 \gamma_\mu$ , and  $\gamma_{5n} = \prod_\mu (\gamma_{5\mu})^{n_\mu}$ .

### 3.2.1 The Naive Fermion Action & The Doubling Problem

The interacting Dirac action is most naively discretised with

$$S_F = \sum_{x,\mu} \bar{\psi}(x) \gamma_\mu \nabla_\mu \psi(x) + m \sum_x \bar{\psi}(x) \psi(x), \quad (3.27)$$

where  $\nabla_\mu$  is the gauge covariant finite difference operator,

$$\nabla_\mu \psi(x) = \frac{1}{2a} \left( U_\mu(x) \psi(x + a\hat{\mu}) - U_\mu^\dagger(x - a\hat{\mu}) \psi(x - a\hat{\mu}) \right). \quad (3.28)$$

$S_F$  is invariant under a so-called *doubling symmetry*, which is generated by

$$\psi(x) \rightarrow \mathcal{B}_\mu \psi(x) \equiv (-1)^{x_\mu/a} \gamma_{5\mu} \psi(x), \quad (3.29)$$

$$\bar{\psi}(x) \rightarrow \bar{\psi}(x) \mathcal{B}_\mu^\dagger \equiv (-1)^{x_\mu/a} \bar{\psi}(x) \gamma_{5\mu}^\dagger. \quad (3.30)$$

The product space of these form a group of 16 elements  $\{\mathcal{B}_\zeta\}$ , labeled by vectors  $\zeta$  with  $\zeta_\mu \in \mathbb{Z}_2$  (e.g. the element  $\mathcal{B}_0 \mathcal{B}_1$  is labeled by  $\zeta = (1, 1, 0, 0)$ ).

The physical significance of this symmetry can be seen when we study its effect on the action. First, notice that

$$\mathcal{B}_\mu \psi(x) = \gamma_{5\mu} \sum_k \tilde{\psi}(k) e^{i(k + \frac{\pi}{a}\hat{\mu}) \cdot x} \quad (3.31)$$

$$= \gamma_{5\mu} \sum_k \tilde{\psi}(k - \frac{\pi}{a}\hat{\mu}) e^{ik \cdot x}, \quad (3.32)$$

where  $\{k\}$  is a discrete set of 4-momenta, with  $k_\mu$  values spaced by  $\pi/aN_\mu$  ( $N_\mu$  = number of sites in direction  $\mu$ ) and truncated at  $\pi/a$ , due to finite size and finite lattice spacing. The action in momentum space can be written as

$$S = \sum_k \bar{\psi}(k) M(k) \tilde{\psi}(k). \quad (3.33)$$

After the operation of  $\mathcal{B}_\mu$  it becomes

$$S \rightarrow \sum_k \bar{\psi}(k) \gamma_{5\mu} M(k + \frac{\pi}{a} \hat{\mu}) \gamma_{5\mu} \tilde{\psi}(k). \quad (3.34)$$

Since we know  $S$  is invariant under this transformation, it must be true that  $\gamma_{5\mu} M(k + \frac{\pi}{a} \hat{\mu}) \gamma_{5\mu} = M(k)$ , and therefore

$$M^{-1}(k + \frac{\pi}{a} \hat{\mu}) = \gamma_{5\mu} M^{-1}(k) \gamma_{5\mu}. \quad (3.35)$$

This is the doubling problem.  $M^{-1}$  is the momentum space propagator for the fermion field, so (3.35) shows that the spectrum of the fermion is periodic, with a period of  $\pi/a$ . We expect a pole in  $M^{-1}(k)$  where  $k \sim m$ ,  $m$  is the pole mass of the fermion. But due to (3.35) there will now be a second pole at  $m + \pi/a$ .

Generalizing this argument to all elements of the doubling symmetry, we see that

$$M^{-1}(k + \frac{\pi}{a} \zeta) = \gamma_{5\zeta} M^{-1}(k) \gamma_{5\zeta}. \quad (3.36)$$

This leads to 16 poles in the fermion spectrum, one for each  $\zeta$  choice, therefore 16 distinct excitations (called *tastes*).

One can isolate a single taste by a block-scaling procedure;

$$\psi^{(\zeta)}(x_B) = \frac{1}{16} \sum_{\delta x_\mu \in \mathbb{Z}_2} \mathcal{B}_\zeta(x_B + \delta x) \psi(x_B + \delta x). \quad (3.37)$$

For example, for  $\zeta = 0$ , it would only contain the original non-doubler taste, since all other poles at  $|k| \sim \pi/a$  have been integrated out. For  $\zeta \neq 0$ , the  $\mathcal{B}_\zeta$  operator pushes the  $\zeta$  doubler to where the  $\zeta = 0$  taste originally was in  $k$  space, then the blocking procedure integrates out the rest.

### 3.2.2 Staggered Quarks

There are a number of solutions to this problem. The most straightforward is to modify the action to push the mass of the unwanted tastes above the momentum cutoff, preventing it from influencing the dynamics, these are called *Wilson-type fermions* [59]. However, actions of this type explicitly break Chiral symmetry.

Among other issues, this causes additive renormalization of the fermion mass, immensely complicating renormalization procedures.

Another approach, known as *staggered fermions* [60], partially resolves the doubling issue while retaining a remnant chiral symmetry. The work presented in this thesis makes extensive use of the staggered formalism.

Staggered fermions are defined via the following. Redefine the fields according to

$$\psi(x) = \gamma_x \chi(x). \quad (3.38)$$

In terms of the new spinor variables  $\chi(x)$ , the naive action (3.27) becomes

$$S_F = \sum_{x,\mu} \bar{\chi}(x)(\alpha_\mu(x)\nabla_\mu + m)\chi(x) \quad (3.39)$$

where  $\alpha_\mu(x) = (-1)^{\sum_{\nu < \mu} x^\mu/a}$ . The action is now diagonal in spin, leading to 4 decoupled grassman variables with identical actions and identical coupling to the gauge field. As a result,  $\chi$  propagators (on fixed gauge backgrounds) are spin diagonal:

$$M_\chi^{-1}(x, y) = g(x, y) \mathbf{1}_{\text{spin}}, \quad (3.40)$$

where  $g(x, y)$  is a singlet under spin. One need only to include a single component of  $\chi$  in a simulation (i.e. fix  $\chi = (\chi_1, 0, 0, 0)$ ). Then they can compute  $M_\chi^{-1}(x, y)[U]$  to obtain  $g(x, y)$ . Then, using the inverse of (3.38),  $g(x, y)$  can be transformed to a propagator of the original spinors:

$$M_\psi^{-1}(x, y) = g(x, y) \gamma_x \gamma_y^\dagger. \quad (3.41)$$

This is clearly computationally beneficial. But also, by shaving off the other spinor components, one reduces the number propagating degrees of freedom by a factor of 4, cutting the number of tastes from 16 down to 4.

We can show more explicitly how this happens. To do this, consider rewriting an isolated taste (3.37) in the staggered formalism, i.e., in terms of  $\chi$ ;

$$\psi^{(\zeta)}(x_B) = \frac{1}{16} \sum_{\delta x_\mu \in \mathbb{Z}_2} \gamma_{\delta x} \mathcal{B}_\zeta(0) \chi(x + \delta x). \quad (3.42)$$

Recall we set  $\chi(x) = (\chi_1(x), 0, 0, 0)$ . The product  $\gamma_{\delta x} \mathcal{B}_\zeta(0)$  is simply a product of gamma matrices, so can only serve to “scramble” the elements of  $\chi$ . Then, in the staggered formalism, all 16 tastes  $\psi^{(\zeta)}$  amount to only 4 distinguishable fermions:  $(\chi_1, 0, 0, 0)$ ,  $(0, \chi_1, 0, 0)$ ,  $(0, 0, \chi_1, 0)$ ,  $(0, 0, 0, \chi_1)$  (with factors of  $(-1)$  and  $i$ ).

In practice in lattice calculations, the remaining multiplicity is tacked in 3 steps:

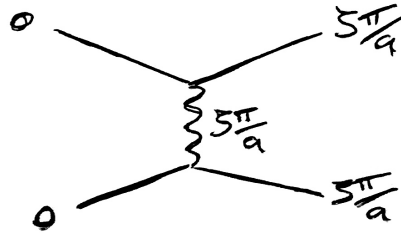


Figure 3.5: Taste mixing at tree level.

1. Ensure only one taste is created and destroyed in the propagator.
2. Minimize the interaction between tastes by a modification of the action.
3. Remove contributions of extra tastes in the fermion sea by taking  $\det M \rightarrow \sqrt[4]{\det M}$  (the context required to understand this step is elucidated in chapter 4).

### 3.2.3 Highly Improved Staggered Quarks

Step 2 above is the guiding principle for the action we use in much of this work, the Highly Improved Staggered Quark (HISQ) action [61].

Interaction between different tastes (“taste mixing”) is dominated by the process in fig. 3.5, the exchange of single gluons carrying momenta close to  $\zeta\pi/a$ . In HISQ, this is suppressed by modifying the gauge fields in such a way as to minimize the coupling between a gluon with momentum  $\zeta\pi/a$  and the fermions, in other words, minimize the vertices in fig. 3.5.

To this end, one can change the action so that fermions only couple to *smeared* gauge links, in which high-frequency excitations have been removed. Define the first and second covariant derivative operators;

$$\begin{aligned} \delta_\rho U_\mu(x) &\equiv \frac{1}{a} (U_\rho(x) U_\mu(x + a\hat{\rho}) U_\rho^\dagger(x + a\hat{\mu}) \\ &\quad - U_\rho^\dagger(x - a\hat{\rho}) U_\mu(x - a\hat{\rho}) U_\rho(x - a\hat{\rho} + a\hat{\mu})), \end{aligned} \quad (3.43)$$

$$\begin{aligned} \delta_\rho^{(2)} U_\mu(x) &\equiv \frac{1}{a^2} (U_\rho(x + a\hat{\rho}) U_\rho^\dagger(x + a\hat{\mu}) \\ &\quad - 2U_\mu(x) \\ &\quad + U_\rho^\dagger(x - a\hat{\rho}) U_\mu(x - a\hat{\rho}) U_\rho(x - a\hat{\rho} + a\hat{\mu})). \end{aligned} \quad (3.44)$$

With this we can define the smearing operator;

$$\mathcal{F}_\mu = \prod_{\rho \neq \mu} \left( 1 + \frac{a^2 \delta_\rho^{(2)}}{4} \right). \quad (3.45)$$

HISQ uses two different smeared gauge fields defined by

$$X_\mu(x) \equiv \mathcal{U} \mathcal{F}_\mu U_\mu(x), \quad (3.46)$$

$$W_\mu(x) \equiv \left( \mathcal{F}_\mu - \sum_{\rho \neq \mu} \frac{a^2 (\delta_\rho)^2}{2} \right) \mathcal{U} \mathcal{F}_\mu U_\mu(x). \quad (3.47)$$

where  $\mathcal{U}$  is a re-unitarization operator, that acts on a matrix  $A$  like  $\mathcal{U}A = A/\sqrt{A^\dagger A}$ .

The HISQ action can then be written as:

$$S_{\text{HISQ}} = \sum_x \bar{\psi}(x) \left( \gamma_\mu \left( \nabla_\mu(W) - \frac{a^2}{6} (1 + \epsilon_{\text{Naik}}) \nabla_\mu^3(X) \right) + m \right) \psi(x) \quad (3.48)$$

Where  $\nabla_\mu(Z)$  is the covariant derivative (3.28) with gauge links replaced with  $Z$ . This action in fact not only removes tree level interactions like fig. 3.5, but also all taste mixing interactions at 1-loop.

The  $\nabla_\mu^3$  term is a Symanzik improvement, it reduces the size of discretisation effects of observables computed using this action. The value of  $\epsilon_{\text{Naik}}$  is fixed according to the constraint

$$\lim_{\underline{p} \rightarrow 0} \frac{E^2(\underline{p}) - m^2}{\underline{p}^2} = 1. \quad (3.49)$$

where  $E(\underline{p})$  obeys the tree-level dispersion relation from the HISQ action. Tuning  $\epsilon_{\text{Naik}}$  according to this constraint gives us the expression

$$\begin{aligned} \epsilon_{\text{Naik}} &= \frac{4 - \sqrt{4 + 12 \frac{m_{\text{tree}}}{\cosh(m_{\text{tree}}) \sinh(m_{\text{tree}})}}}{\sinh^2(m_{\text{tree}}) - 1}, \\ m_{\text{tree}} &= m \left( 1 - \frac{3}{80} m^4 + \frac{23}{2240} m^6 + \frac{1783}{537600} m^8 \right. \\ &\quad \left. - \frac{76943}{23654400} m^{10} \right) + \mathcal{O}(m^{12}). \end{aligned} \quad (3.50)$$

### 3.3 Heavy Quarks on the Lattice

The range of different quark masses in nature present a number of further complications to lattice calculations.  $u$  and  $d$  quarks cause huge problems due to how light they are, this will be addressed in Sec. 4.1.2.  $s$  quarks are easy.

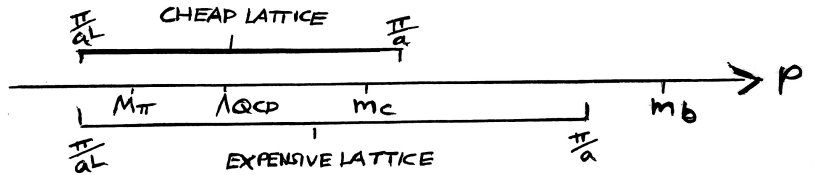


Figure 3.6: Different scales relevant to non-perturbative physics, and brackets showing the range of scales that typical lattices can resolve. The larger the range of scales resolved, the more computationally expensive the calculation.

As quarks get heavier, we begin to encounter another problem. Discretisation effects will generally grow like the largest scale in the theory. If the observable being computed on the lattice is sensitive to the dynamics of a heavy quark of mass  $m_h$ , this will contain discretisation effects of size  $(am_h)^n$  (where  $n$  depends on how improved the action is). This is essentially due to the de Broglie wavelength of the heavy quark excitations being close to the lattice spacing, the excitations 'hide' in-between lattice sites.

How heavy we can go is limited to two factors: the improvement of the lattice action and the lattice spacing. How fine we can get the lattice spacing is limited by computational cost. The physical size of the lattice must always be at least large enough to fit the lightest degrees of freedom in the system, namely it must be larger than the wavelength of pions. This means to get smaller lattice spacing requires increasing the number of sites on the lattice, hence increasing the computational costs (details in chapter 4).

In the past,  $c$  quarks resulted in uncontrollable discretisation effects, but now armed with highly improved actions like HISQ, and very fine lattices,  $c$  physics has been conquered on the lattice [62–68].

The mass of the  $b$  is still somewhat out of reach. Even with the HISQ action and the finest lattices available with current computational constraints, physical  $b$  quarks will create uncontrollable discretisation effects.

The work in this thesis concerns the decays of mesons containing  $b$  quarks. We approach the issue of the heavy  $b$  in two different ways, the *heavy-HISQ* approach, and the *Lattice NRQCD* action. Since the main results of this thesis result from our heavy-HISQ studies, we will not go into too much detail in describing lattice NRQCD.

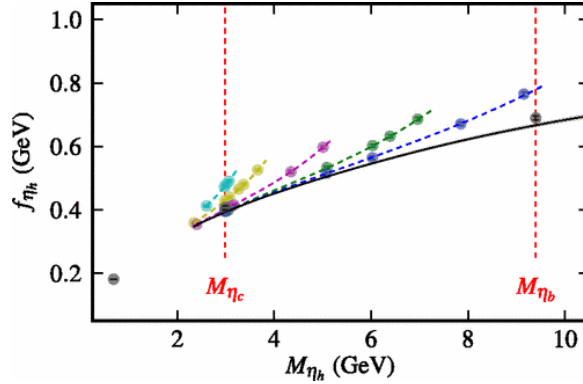


Figure 3.7: An extrapolation to  $m_h = m_b$  of the  $\eta_h$  decay constant (where  $\eta_h$  is a pseudoscalar  $\bar{h}h$  meson [69]). The colourful points are measurements of  $f_{\eta_h}$  on the lattice, the colour denotes lattice spacing. The  $x$  axis,  $M_{\eta_h}$ , is a proxy for the  $h$ -quark mass.

### 3.3.1 Heavy HISQ

The heavy-HISQ approach is essentially to model the  $b$  with the HISQ action, but to perform the calculation at a number of unphysically light  $b$  masses (that we refer to generically as heavy  $h$  quarks), and extrapolate the results to the physical  $b$  mass. Typically the  $h$  masses span most of the region between the  $c$  mass and the  $b$  mass.

Luckily there exists an effective field theory for understanding how to perform such an extrapolation - HQET. HQET gives a framework to describe how observables depend on masses of heavy quarks, so one can use HQET to derive fit forms of such an extrapolation.

The heavy-HISQ approach is a reasonably new program. It has so far been used for computing  $b$  decay constants and masses [69], and a number of heavy-HISQ calculations of semileptonic form factors are currently underway. The work presented in chapters 6 and 7 adopt the heavy-HISQ approach for computing  $B_s \rightarrow D_s^* l \nu$  and  $B_s \rightarrow D_s l \nu$  form factors. Besides these, there are also currently ongoing calculations of form factors for the  $B_c \rightarrow \eta_c l \nu$ ,  $B_c \rightarrow J/\psi l \nu$  [70],  $B_c \rightarrow B_s l \nu$ ,  $B_s \rightarrow \eta_s l \nu$ , and  $B \rightarrow D^* l \nu$  decays.

### 3.3.2 Lattice NRQCD

The root of the problem of heavy quarks on the lattice is in the rest mass of the quark. Consider the expansion in momentum  $\mathbf{p}^2$  of the continuum relativistic dispersion

relation:

$$\omega = \sqrt{\mathbf{p}^2 + m^2} \simeq m + \frac{\mathbf{p}^2}{2m} - \frac{\mathbf{p}^4}{4m^3} + \dots \quad (3.51)$$

the first term (rest mass) is the source of the issue, when  $m > 1/a$  the first term pushes the frequency of excitations  $\omega$  close to or over  $\pi/a$ .

Another solution to heavy quarks is to replace the relativistic fermion action e.g. HISQ, with a lattice version of NRQCD [53]. In NRQCD the  $b$  has no rest mass.

Another benefit of NRQCD is that it does not suffer from a doubling problem, since the doubling problem is a purely relativistic issue (the doubling symmetry requires 4 component spinors for  $\gamma$  matrices to act on).

The lattice calculations we perform require us to compute propagators for  $b$  quarks on fixed gauge backgrounds. The form of the action allows propagators  $M^{-1}[U]$  to be computed using a simple recursion relation

$$M_b^{-1}(\mathbf{x}, t+1)[U] = e^{-aH}[U]M_b^{-1}(\mathbf{x}, t)[U], \quad (3.52)$$

which is numerically very fast.  $H$  is the NRQCD Hamiltonian. In the interest of numerical stability, the time evolution operator is re-cast as

$$e^{-aH} = \left(1 - \frac{a\delta H}{2}\right) \left(1 - \frac{aH_0}{2n}\right)^n U_0^\dagger(\mathbf{x}, t) \left(1 - \frac{aH_0}{2n}\right)^n \left(1 - \frac{a\delta H}{2}\right), \quad (3.53)$$

where  $n$  is an arbitrary integer (chosen in our studies to be  $n = 4$ ), and the Hamiltonian has been broken up into a leading part  $H_0$  and correction  $\delta H$ . We use the  $\mathcal{O}(\alpha_s v^4)$  corrected NRQCD Hamiltonian:

$$\begin{aligned} aH_0 &= -\frac{\nabla^{(2)}}{2am_b}, \\ a\delta H &= -c_1 \frac{(\nabla^{(2)})^2}{8(am_b)^3} + c_2 \frac{i}{8(am_b)^2} (\nabla \cdot \tilde{\mathbf{E}} - \tilde{\mathbf{E}} \cdot \nabla) \\ &\quad - c_3 \frac{1}{8(am_b)^2} \sigma \cdot (\nabla \times \tilde{\mathbf{E}} - \tilde{\mathbf{E}} \times \nabla) \\ &\quad - c_4 \frac{1}{2am_b} \sigma \cdot \tilde{\mathbf{B}} + c_5 \frac{\nabla^{(4)}}{24am_b} \\ &\quad - c_6 \frac{(\nabla^{(2)})^2}{16n(am_b)^2} \end{aligned} \quad (3.54)$$

where  $\nabla^{(2,4)}$  are the second and fourth lattice derivative,  $\tilde{\mathbf{E}}$  and  $\tilde{\mathbf{B}}$  are the (Symmanzik improved) chromoelectric and chromomagnetic fields. The form of  $\nabla^{(2,4)}, \tilde{\mathbf{E}}, \tilde{\mathbf{B}}$  are defined in sec. 4.2 of [53], and were improved upon in [71].

The coefficients  $\{c_i\}$  have been fixed via various calculations adopting a number of methods. The coefficients of the kinetic terms,  $c_{1,5,6}$ , were most recently fixed by comparing the lattice NRQCD dispersion relation to that of the continuum in perturbation theory [72].  $c_2$  is a spin-independent term which can effect radial and orbital excitation energies, this is not expected to have as large an effect as the kinetic terms, so is set to its tree-level value of 1. The result of varying  $c_2$  on relevant observables was investigated in Sec. IIIC of [73], and the effects were very small.  $c_3$  and  $c_4$  are spin-dependent terms, which would have a small effect on spin-averaged observables (i.e. all observables computed in this work).  $c_3$  is set to 1, and  $c_4$  is tuned non-perturbatively, by matching predictions of the fine structure of the  $\Upsilon$  spectrum from lattice NRQCD to experiment [73].

Once the propagator for the 2-component non-relativistic  $b$  quark has been found, it must be transformed back into a 4-component spinor. This is done by an inverse Fouldy-Wouthuysen transformation [52]

$$\psi(x) = e^{-\frac{\gamma \cdot \mathbf{D}}{2m_b}} \begin{pmatrix} \psi_+(x) \\ 0 \end{pmatrix}. \quad (3.56)$$



## CHAPTER 4

# Lattice Calculations

---

The last chapter focused on how to discretize QCD on a lattice. This chapter is focused on the practical side of lattice QCD - given a lattice action, how does one perform the functional integral to determine expectation values of operators.

### 4.1 Evaluating Lattice Correlation Functions

All physics of a quantum field theory can be extracted from correlation functions. So a typical lattice calculation involves computing a correlation function (or just *correlator*) on the lattice, then extracting physical quantities from it. A typical correlator that is computed on the lattice is a 2-point meson correlator, i.e. when  $\mathcal{O} = \Phi(x)\Phi^\dagger(y)$  and  $\Phi$  is a meson creation operator. This is a good working example for showing the steps in a lattice calculation, the generalization to  $N$ -point correlators is reasonably natural.

A creation operator for a meson in this context can be any operator containing the same quantum numbers as the meson one studying. For example, the neutral  $B$  meson is a pseudoscalar charged with a  $d$  and  $\bar{b}$  quark, so a suitable operator is  $\Phi(x) = \bar{b}(x)\gamma_5 d(x)$ . The corresponding functional can then be written as

$$C(x, y) = \langle \Phi(x)\Phi^\dagger(y) \rangle = \int [d\psi d\bar{\psi} dU] (\bar{b}(x)\gamma_5 d(x)\bar{d}(y)\gamma_5 b(y)) \\ \times \exp \left( -S_G[U] - \sum_{w,z,i} \bar{q}_i(w) M_{q_i}(w, z)[U] q_i(z) \right), \quad (4.1)$$

where we have broken the action up into a gauge part  $S_G[U]$ , and a fermion part.  $M_{q_i}(x, y)[U]$  is the Dirac operator for flavour  $i$ , and can be seen as a matrix in lattice site, color and spin.

The integral over fermions can be performed analytically since the fermion fields

are Grassman valued. In our example, the result is [74];

$$\begin{aligned} C(x, y) = & \int [dU] \text{Tr} \left( M_b^{-1}(y, x)[U] \gamma_5 M_d^{-1}(x, y)[U] \gamma_5 \right) \\ & \times e^{-S_G[U]} \prod_i \det(M_{q_i}[U]). \end{aligned} \quad (4.2)$$

The quantities  $M_{q_i}^{-1}(x, y)[U]$  are propagators of a quark of flavour  $q$  on a fixed gauge background  $U$ . Here  $U$  denotes a configuration of angles comprising an  $SU(3)$  matrix for each element of the set of all links on the lattice  $\{U_\mu(x) | \forall \mu, x\}$ . The trace is over color and spin. The integration over gauge fields is generally carried out by an importance sampling method. A finite *ensemble* of gauge configurations  $\{U_n\}$  is generated by a Monte Carlo Markov Chain (MCMC), where the probability of a gauge configuration  $U_n$  being added to the ensemble is proportional to

$$p(U_n) = e^{-S_G[U_n]} \prod_i \det(M_{q_i}[U_n]). \quad (4.3)$$

Once the ensemble is created, the path integral can be approximated by simply

$$C(x, y) \simeq \frac{1}{N} \sum_n \text{Tr} \left[ M_b^{-1}(y, x)[U_n] \gamma_5 M_d^{-1}(x, y)[U_n] \gamma_5 \right] \quad (4.4)$$

where  $N$  is the size of the ensemble. The calculation of the correlation function then is split into 3 steps:

1. Generate an ensemble of Gauge configurations  $\{U_i\}$  by MCMC (sec. 4.1.1).
2. Compute  $M_{q_i}^{-1}(x, y)[U]$  by inverting the Dirac operator on each Gauge configuration (sec. 4.1.2).
3. Construct trace as in (4.4), and average over the ensemble. This step is dealt with in the context of staggered quarks in 4.1.3.

#### 4.1.1 Generation of Gauge Ensembles

The calculation requires a number of samples of gauge configurations  $\{U_n\}$  sampled from the distribution  $p(U)$  defined in (4.3).

The physical interpretation of the determinant in (4.3) is that it accounts for virtual quark loops in the Dirac sea. In the early days of lattice calculations, this determinant was approximated to 1, since its presence caused an insurmountable computational cost, and it was expected that sea quarks had small effects on observables (this is known as the *quenched approximation*). These days, our computational

ability has improved and sophisticated approaches to the determinant have been developed, so we can include it in our calculations.

We will roughly follow the history of gauge ensemble generation, by first ignoring the determinant, and then showing how it is eventually included in the process.

### Quenched MCMC

Gauge ensembles are generated via an MCMC, inspired by statistical mechanics. The distribution  $\exp(-S_G[U])$  is suggestive of something like a Boltzmann distribution for a gas of particles, each with some state  $U_i$ , in thermal equilibrium. The ergodic hypothesis states that a single particle in this gas will jump between possible states over time such that, at any given time, its probability of being in state  $U_i$  is given by  $\exp(-S_G[U_i])$ . In MCMC, one starts with some random state  $U_0$ , then repeatedly updates the state according to some update 'hopping rate'  $p(U_i \rightarrow U_j)$ . This results in a list of states that appear sampled from the distribution  $\exp(-S_G[U])$ .

The hopping rate must be designed to bring the chain into thermal equilibrium with the correct distribution. A sufficient condition for thermal equilibrium is so-called *detailed balance*, where the probability of jumps between any pair of states  $i$  and  $j$  is equal:

$$p(U_i)p(U_i \rightarrow U_j) = p(U_j)p(U_j \rightarrow U_i). \quad (4.5)$$

Hence  $p(U_i \rightarrow U_j)$  must be designed according to the rule

$$\frac{p(U_i \rightarrow U_j)}{p(U_j \rightarrow U_i)} = \exp(-(S_G[U_i] - S_G[U_j])). \quad (4.6)$$

There are a number of possible choices of how to design  $p(U_i \rightarrow U_j)$ . One approach, known as **molecular dynamics** [75, 76] is to model the chain as the trajectory  $U(\tau)$  of a system with hamiltonian

$$H(\pi, U) = \frac{\pi^2}{2} + S_G[U], \quad (4.7)$$

where  $\pi$  is a fictitious momentum conjugate to  $U$ . It can be demonstrated that such a trajectory obeys (4.6). The trajectory is computed via Runge-Kutta methods. To deal with the possibility of fixed points, limit cycles etc. in the dynamics (which would prevent ergodicity), one can introduce a periodic **refreshing** step, where  $\pi$  assigned a new value from normally distributed noise [77, 78].

Another problem that can occur in molecular dynamics is when errors in Runge-Kutta iterations accumulate over time. Diversion from the dynamics enforced by  $H(\pi, U)$  can ruin the ergodicity of the trajectory. To fix this, one can add a **Metropolis** step at regular intervals  $\delta\tau$  throughout the evolution [79]. In this step, one either accepts (continues onto the next stage of molecular dynamics) or rejects (refreshes  $\pi$  and re-calculates the last stage of molecular dynamics), according to the criterion

- If  $S_G[U(\tau + \delta\tau)] < S_G[U(\tau)]$ , always accept
- Otherwise, accept if  $\exp(S_G[U(\tau + \delta\tau)] - S_G[U(\tau)]) > \lambda$ , where  $\lambda$  is randomly chosen from the interval  $[0, 1]$ .

The metropolis step ensures (4.6) is satisfied even in the presence of Runge-Kutta errors.

The combination of molecular dynamics, refreshing steps and Metropolis steps is referred to as **Hybrid Monte Carlo** [80], and is the basic structure of how the ensembles we use in this thesis were generated. We now address how the determinant  $\det M$  is included.

### Unquenched MCMC

Simply evaluating  $\det M[U]$  directly, given a configuration  $U$ , is prohibitively expensive due to the non-local nature of the determinant (recall  $M[U]$  is a matrix in spin, colour, and lattice site, in modern calculations this will have a dimension of order  $10^8$ .) A solution to this is to use the  $\Phi$ -algorithm [81].

First, we replace  $\det M$  with  $\det M^\dagger M$ . If we were only including  $u$  and  $d$  quarks in the sea, this would be fine since we can approximate  $u$  and  $d$  to be two degenerate flavours, then  $\prod_q \det M_q = \det M \det M = \det M^\dagger M$ . In the case of an arbitrary set of flavours, this requires a correction that will be addressed later. This involves introducing new scalar fields  $\Phi(x)$  and  $\Phi^\dagger(x)$  via

$$\det M^\dagger M = \int [d\Phi^\dagger d\Phi] \exp(-\Phi^\dagger (M^\dagger M)^{-1} \Phi). \quad (4.8)$$

then one can add  $-\Phi^\dagger (M^\dagger M)^{-1} \Phi$  to  $S_G$  in the Hybrid Monte Carlo algorithm. The extra functional integral over  $\Phi, \Phi^\dagger$  is easily evaluated, by sampling a vector  $\eta$  from a normal distribution  $\exp(-\eta^\dagger \eta)$ , then transforming it to  $\Phi = M^\dagger \eta$ .

### The Dreaded Rooting Procedure

We will now address how to correct for the fact that we have replaced  $\det M$  with  $\det M^\dagger M$  in the presence of arbitrary non-degenerate flavours. We have explicitly doubled the fermions to two degenerate flavours per physical flavour. In the case of staggered quarks, this is not a huge deal since we already have four degenerate tastes which we have to deal with anyway. As mentioned in Sec. 3.2.2, in order to cut down the number of tastes in the sea, the solution is to take the fourth-root of  $\det M$ . When using the  $\Phi$ -algorithm, this becomes the 8-th root of  $\det M^\dagger M$ .

$$\begin{aligned} (\det M^\dagger M)^{1/8} &= \left(\prod_i \lambda_i^2\right)^{1/8} = \left(\prod_i \lambda_i\right)^{1/4} \\ &\stackrel{?}{=} \left(\prod_i \lambda'_i{}^4\right)^{1/4} = \prod_i \lambda'_i \quad (a \rightarrow 0). \end{aligned} \tag{4.9}$$

where  $\lambda_i$  are eigenvalues of  $M$ . On the second line, we have assumed that the matrix  $M$  can be decomposed into four matrices for each of the four tastes, with eigenvalues  $\lambda'_i$  which are degenerate in the continuum limit.

This assumption is not rigorously justified in field theory, so the fourth-root trick is a source of much controversy, and is the main objection to staggered quarks [82–84]. There has so far emerged no evidence that this is harmful, since all observables ever computed from the staggered quark formalism have agreed with experiment, analytical approaches, and other lattice discretisations. The empiricists among us would say this is evidence for the validity of the fourth-root trick.

Introducing the 1/2 or 1/8th root to the determinant requires a modification of the  $\Phi$  algorithm, we can no longer simply sample  $\Phi$  using  $\Phi = M^\dagger \eta$ . The effective action is now  $S_G + \Phi^\dagger (M^\dagger M)^{-1/8} \Phi$ . The root is dealt with by replacing it with a partial fraction representation [85];

$$(M^\dagger M)^{-1/8} \simeq a_0 + \sum_{n=1}^N \frac{a_n}{M^\dagger M + b_n}. \tag{4.10}$$

This can only be evaluated by some variation of a conjugate gradient algorithm (specifically a so-called multishift solver [86, 87]), conjugate gradient will be described in sec. 4.1.2. This approach is called the **Rational Hybrid Monte Carlo** (RHMC) algorithm.

### The $N_f = 2 + 1 + 1$ MILC Ensembles

In this work we use ensembles of gauge configurations generated by the MILC collaboration [88, 89]. The ingredients of these configurations are

set	handle	$a/\text{fm}$	$N_x^3 \times N_t$	$am_{l0}$	$am_{s0}$	$am_{c0}$
0	<b>very coarse</b>	0.1543(8)	$16^3 \times 48$	0.013	0.067	0.838
1	<b>coarse</b>	0.1241(7)	$24^3 \times 64$	0.0102	0.0509	0.635
2	<b>fine</b>	0.0884(6)	$32^3 \times 96$	0.0074	0.037	0.440
3	<b>fine-physical</b>	0.0873(5)	$64^3 \times 96$	0.0012	0.0363	0.432
4	<b>superfine</b>	0.05922(12)	$48^3 \times 144$	0.0048	0.024	0.286
5	<b>ultrafine</b>	0.04406(23)	$64^3 \times 192$	0.00316	0.0158	0.188

Table 4.1: Parameters for gluon ensembles [88,89].  $a$  values for sets 0-3 were deduced in [90], set 4 from [91]. We thank C. McNeile for computing the  $a$  value on set 5. These  $a$  values are determined by measuring the Wilson flow parameter  $w_0/a$  on the lattice, then using the known value for  $w_0$  to isolate  $a$ . Columns 5-7 give the masses used in the action for light, strange and charm quarks in the sea.

- Gauge fields obeying the one-loop Symanzik improved Lüscher-Weitz action described in Sec. 3.1.2.
- Four flavours of quark in the sea,  $u,d,s$  and  $c$  (with  $m_u = m_d \equiv m_l$ ), hence the notation  $N_f = 2 + 1 + 1$ , obeying the HISQ action, described in sec. 3.2.3.
- Ensemble generated using the RHMC Algorithm as described earlier in this section.

Table 4.1 gives the details of the MILC ensembles that were used in this work. One may notice that for the majority of ensembles here, the light quarks are obscenely heavier than in reality. The necessity for this is explained in the next section.

#### 4.1.2 Dirac Operator Inversion

Once the ensemble  $\{U_i\}$  has been generated, to compute the 2-point correlator (4.4) one must compute  $M^{-1}[U_i]$  for each  $U_i$ . We have already seen how this can be done in the case of the flavour in question being governed by the NRQCD action, one can use the recursion relation (3.52). In the case of relativistic actions like HISQ, there is no equivalent recursion relation.

$M$  is large but sparse, it technically has  $\mathcal{O}(\text{Vol}^2)$  elements, but for suitably local actions (like HISQ) it has only  $\mathcal{O}(\text{Vol})$  non-zero elements. This means it is well-

suites to the **conjugate gradient** (CG) algorithm [92] (and it's variants), which has become the most successful approach to computing  $M^{-1}$ . However, CG requires the matrix being inverted to be hermitian and positive definite, which is not necessarily the case for  $M$ . We instead invert  $M^\dagger M$ , which is hermitian and positive definite, then we can recover  $M^{-1}$  by acting  $M^\dagger$  on  $(M^\dagger M)^{-1}$ .

The design of CG requires a bunch of explanation which we will not go into here. We will instead briefly describe the philosophy behind it, and state the algorithm. The goal is, given some vector  $b$  and matrix  $A$ , to find  $x$  where

$$Ax = b. \quad (4.11)$$

In our case  $A = M^\dagger M$  and  $b$  is a suitably chosen 'source' for the propagator (see sec. 4.1.3). This is equivalent to finding the  $x = x^*$  that minimizes

$$f(x) = b^T Ax - b^T b. \quad (4.12)$$

A reasonable solution to this problem is something like a *steepest descent* approach, where one starts at a random  $x_0$ , then moves some distance  $\alpha_0$  in the direction  $r_0 = x^* - x_0 = b - Ax_0$  to  $x_1 = x_0 - \alpha_0 r_0$ , where  $\alpha_0$  is chosen to minimize  $r_1 = x^* - x_1$ . And then repeat. This approach has the property that each new step  $\alpha_n r_n$  is orthogonal to every other step, this means the algorithm takes a sub-optimal zig-zag path towards the solution.

CG is designed to take a more direct path, by imposing the condition that the direction of each step  $d_n = (x_n - x_{n-1})/\alpha_n$  is orthogonal with respect to the metric  $A$ , i.e.  $d_n^T A d_m = 0$  for  $n \neq m$ . The CG algorithm is

$$\begin{aligned} x_{n+1} &= x_n + \alpha_n d_n, \text{ where} \\ \alpha_n &= \frac{r_n^T r_n}{d_n^T A d_n}, \\ d_n &= \begin{cases} r_0, & n = 0 \\ r_n + \beta_n d_{n-1}, & n > 0, \end{cases} \\ r_n &= b - Ax_n, \\ \beta_n &= \frac{r_n^T r_n}{r_{n-1}^T r_{n-1}}. \end{aligned} \quad (4.13)$$

One terminates the algorithm when some stopping condition is achieved, namely when  $r_n < \epsilon$  where  $\epsilon$  is some small number referred to as the error tolerance, or when some maximum number of iterations has been reached.

The complexity of the CG algorithm is  $\mathcal{O}(c)$  where  $c = \lambda_{\max}/\lambda_{\min}$  is the condition number of the matrix  $A$  ( $\lambda_{\max/\min}$  are the largest and smallest eigenvalues of  $A$ ). The condition number quantifies the size of rounding errors that accumulate in iterative processes like CG. In our case where  $A = M^\dagger M \sim (-iD + m)(iD + m)$ , the condition number is proportional to  $m^{-2}$ . Hence, propagators for lighter quarks are quadratically more expensive to compute than heavier ones. This not only effects the computation of correlation functions between light quarks via  $M^{-1}$ , but any unquenched calculation with rooting since in that case we must also invert (4.10).

For this reason, lattice calculations are often computed with unphysically heavy  $u/d$  quarks. When computing observables that are sensitive to the light quark masses, modern lattice calculations have measured the observable for a number of light quark masses and extrapolated downwards to the physical light mass, using chiral perturbation theory as a guide. In the MILC ensembles we use in this work, summarized in table 4.1, all but one have a light mass at around  $m_l/m_s \simeq 1/5$ , while set 3 has roughly physical light quarks at  $m_l/m_s \simeq 1/30$ .

### 4.1.3 Staggered Correlation Functions

We now turn to how to evaluate traces of quark propagators like in (4.2), specifically in the staggered formalism.

Recall  $\psi$ -propagators  $M^{-1}$  are related to  $\chi$ -propagators  $g$  by

$$M^{-1}(x, y) = \gamma_x \gamma_y^\dagger g(x, y). \quad (4.14)$$

Throughout this section we will keep the  $U$ -dependence of  $M^{-1}$  and  $g$  implicit. By conjugating both sides and using the property of the naive propagator  $(M^{-1})^\dagger(x, y) = \gamma_5 M^{-1}(y, x) \gamma_5$  (known as  $\gamma_5$ -hermiticity) one can show that  $M^{-1}$  can also be written as

$$M^{-1}(x, y) = \phi_5(x) \phi_5(y) \gamma_x \gamma_y g^\dagger(y, x), \quad (4.15)$$

where  $\phi_5(x) = (-1)^{\sum_\mu x_\mu}$ .

## 2-point correlation functions

Consider the generic 2-point correlator:

$$\begin{aligned} C(x, y) &= \langle \Phi_X^\dagger(x) \Phi_Y(y) \rangle_{\psi, U} , \quad \Phi_X(x) = \frac{1}{4} \bar{\psi}_a(x) \gamma_X \psi_b(x) \\ &= \frac{1}{16} \langle \text{Tr}_{c,s} \gamma_X M_a^{-1}(x, y) \gamma_Y M_b^{-1}(y, x) \rangle_U \\ &= \frac{1}{16} \text{Tr}_s \left( \gamma_x^\dagger \gamma_X \gamma_x \gamma_y^\dagger \gamma_Y \gamma_y \right) \langle \text{Tr}_c (M_a^{-1}(x, y) M_b^{-1}(y, x)) \rangle_U \end{aligned} \quad (4.16)$$

$\text{Tr}_s$  is a trace over spin and  $\text{Tr}_c$  is over colour. To deal with the spin trace, define the family of phases  $\{\phi_X(x)\}$  according to

$$\gamma_x^\dagger \gamma_X \gamma_x = \phi_X(x) \gamma_X. \quad (4.17)$$

for example, if  $X = 5$ , then  $\gamma_x^\dagger \gamma_5 \gamma_x = (-1)^{\sum_\mu x_\mu} \gamma_x^\dagger \gamma_x \gamma_5 = \phi_5(x) \gamma_5$ . The map from  $X$  to  $\phi_X$  is structure preserving, i.e. if  $\gamma_X = \gamma_A \gamma_B$ , then  $\phi_X(x) = \phi_A(x) \phi_B(x)$ . The spin trace becomes  $\phi_X(x) \phi_Y(y) \text{Tr}_s(\gamma_X \gamma_Y)$ . The remaining trace will vanish unless  $Y = X$ , and is 4 otherwise. We end up with

$$C(x, y) = \frac{1}{4} \phi_{5X}(x) \phi_{5X}(y) \langle \text{Tr}_c g_a(x, y) g_b^\dagger(x, y) \rangle_U, \quad (4.18)$$

where we have applied (4.15) to  $M_b^{-1}$  and  $\phi_{5X}(x) = \phi_5(x) \phi_X(x)$ . To obtain the correlation function of a meson in a momentum eigenstate with spacial momentum  $\mathbf{p}$ , the above must be replaced with

$$\begin{aligned} C_{\mathbf{p}}(t_0, t) &= \frac{1}{N_x^3} \sum_{\mathbf{x}, \mathbf{y}} e^{i\mathbf{p} \cdot (\mathbf{x} - \mathbf{y})} C(\mathbf{x}, t_0; \mathbf{y}, t) \\ &= \frac{1}{4N_x^3} \sum_{\mathbf{x}, \mathbf{y}} e^{i\mathbf{p} \cdot (\mathbf{x} - \mathbf{y})} \phi_{5X}(x) \phi_{5X}(y) \langle \text{Tr}_c g_a(x, y) g_b^\dagger(x, y) \rangle_U, \end{aligned} \quad (4.19)$$

where it is understood that  $x_0 = t_0$  and  $y_0 = t$ . In order to evaluate this function, the simulation must perform inversions to create  $g_{a/b}(x, y)$  for each  $x$  and  $y$ , so  $2 \cdot \text{Vol}^2$  operations. This is prohibitively expensive. The number of inversions can be reduced using *random wall sources*. Define

$$P_{a, \mathbf{p}, X}^{t_0}(y) \equiv \frac{1}{\sqrt{N_x^3}} \sum_{\mathbf{x}} e^{i\mathbf{p} \cdot (\mathbf{x} - \mathbf{y})} \phi_{5X}(\mathbf{x}, t_0) \xi(\mathbf{x}) g_a(\mathbf{x}, t_0; y), \quad (4.20)$$

where  $\xi(\mathbf{x})$  is a random field of colour vectors, varying configuration-by-configuration. This has the property

$$\langle f(\mathbf{x}, \mathbf{x}') \xi^*(\mathbf{x}') \xi(\mathbf{x}) \rangle_U = \delta_{\mathbf{x}, \mathbf{x}'} \langle f(\mathbf{x}, \mathbf{x}') \rangle_U. \quad (4.21)$$

Using this property the correlator can be built instead according to

$$C(t_0, t) = \frac{1}{4} \sum_{\mathbf{y}} \phi_{5X}(y) \langle \text{Tr}_c P_{a,\mathbf{p},X}^{t_0}(\mathbf{y}, t) P_{b,0,1}^{t_0}(\mathbf{y}, t) \rangle_U. \quad (4.22)$$

Now all one has to compute is  $P_{a/b}^{t_0}(y)$  for general  $y$ , so 2·Vol operations, a reduction by a factor of Vol.

### 3-point correlation functions

The above discussion can be generalized to 3-(or  $N$ -)point correlation functions using *extended sources*. Consider a 3-point correlation function, for example encoding an  $X \rightarrow Y$  semileptonic decay via a current  $J(y)$ ;

$$\begin{aligned} C(x, y, z) &= \langle \Phi_X^\dagger(x) J(y) \Phi_Z(z) \rangle_{\psi, U} , \quad \Phi_X(x) &= \frac{1}{4} \bar{\psi}_b(x) \gamma_X \psi_s(x) \\ J(y) &= \bar{\psi}_b(y) \gamma_J \psi_a(y) \\ \Phi_Z(z) &= \frac{1}{4} \bar{\psi}_a(z) \gamma_Z \psi_s(z). \end{aligned} \quad (4.23)$$

We can reduce this in the same way as before

$$C(x, y, z) = \frac{1}{16} \text{Tr}_s \left( \gamma_x^\dagger \gamma_X \gamma_x \gamma_y^\dagger \gamma_J \gamma_y \gamma_z^\dagger \gamma_Z \gamma_z \right) \langle \text{Tr}_c g_b(x, y) g_a(y, z) g_s(x, z) \rangle_U \quad (4.24)$$

$$= \frac{1}{4} \phi_{5X}(x) \phi_J(y) \phi_{5Z}(z) \langle \text{Tr}_c g_b(x, y) g_a(y, z) g_s^\dagger(x, z) \rangle_U. \quad (4.25)$$

We have assumed that  $\text{Tr}_s \gamma_X \gamma_J \gamma_Z = 4$ , requiring that each gamma matrix in this combination has a partner and therefore cancels.

Putting  $X$  into an eigenstate of zero momentum, and  $Y$  into an eigenstate of momentum  $\mathbf{p}$ , we get

$$\begin{aligned} C_{\mathbf{p}}(t_0, t, T) &= \frac{1}{4N_x^3} \sum_{\mathbf{x}, \mathbf{y}, \mathbf{z}} e^{i\mathbf{p} \cdot (\mathbf{y} - \mathbf{z})} \phi_{5X}(x) \phi_J(y) \phi_{5Z}(z) \\ &\times \langle \text{Tr}_c g_b(\mathbf{x}, t_0; \mathbf{y}, t) g_a(\mathbf{y}, t, \mathbf{z}, T) g_s^\dagger(\mathbf{x}, t_0; \mathbf{z}, T) \rangle_U. \end{aligned} \quad (4.26)$$

This can be built by first creating propagators for the  $b$  and  $s$  quarks -  $P_{b,0,X}^{t_0}(y), P_{s,0,1}^{t_0}(z)$ . Then, build the  $a$  propagator using an extended source, i.e.:

$$P_{a,\mathbf{p},ext}^T(y) = \sum_{\mathbf{z}} P_{s,0,1}^{t_0}(\mathbf{z}, T) \phi_{5Z}(\mathbf{z}, T) g_a(\mathbf{z}, T; y). \quad (4.27)$$

Then,  $P_{b,0,X}^{t_0}(y)$  and  $P_{a,\mathbf{p},ext}^T(y)$  can be used to construct (4.22), giving a result for the 3-point correlation function.

### Momentum Twist

The momentum space 2-point correlation function for an operator  $\mathcal{O}$  with external momentum  $\mathbf{p}$  is given by

$$C_{\mathbf{p}}(0, t) = \sum_{\mathbf{x}} e^{i\mathbf{p}\cdot\mathbf{x}} \langle \mathcal{O}^\dagger(\mathbf{x}, t) \mathcal{O}(\mathbf{0}, 0) \rangle. \quad (4.28)$$

To extend the method for computing zero momentum correlators to non-zero, one needs to add an appropriate phase to the operators;

$$\mathcal{O}(\mathbf{x}, t) \rightarrow \mathcal{O}(\mathbf{x}, t) e^{-i\mathbf{p}\cdot\mathbf{x}} \quad (4.29)$$

$$\implies C(\mathbf{0}, t) \rightarrow C(\mathbf{p}, t). \quad (4.30)$$

This generalised straightforwardly to  $n$ -point functions. One can assign the rephasing to any factor in  $\mathcal{O}$ , for example a fermion operator

$$\psi(\mathbf{x}, t) \rightarrow \psi(\mathbf{x}, t) e^{-i\mathbf{p}\cdot\mathbf{x}}. \quad (4.31)$$

Rephasing  $\psi$  is equivalent to introducing the so-called *momentum twist* to the gauge links [93]. The action of (4.29) on any gauge invariant quantity is equivalent to

$$U_i \rightarrow U_i e^{ip_i} \quad (\text{no sum}). \quad (4.32)$$

For example consider the effect this has on the following operator

$$\begin{aligned} & \psi^\dagger(x) U_\mu(x) U_\nu(x + a\hat{\mu}) \psi(x + a\hat{\mu} + a\hat{\nu}) \\ & \rightarrow \psi^\dagger(x) (e^{ip_\mu} U_\mu(x)) (e^{ip_\nu} U_\nu(x + a\hat{\mu})) \psi(x + a\hat{\mu} + a\hat{\nu}) \\ & \rightarrow \psi^\dagger(x) e^{-\mathbf{p}\cdot\mathbf{x}} U_\mu(x) U_\nu(x + a\hat{\mu}) e^{-\mathbf{p}\cdot(\mathbf{x} + a\hat{\mu} + a\hat{\nu})} \psi(x + a\hat{\mu} + a\hat{\nu}). \end{aligned} \quad (4.33)$$

(4.32) is how external momenta is simulated in the calculations in this thesis.

## 4.2 Analysis of Correlation Functions

Once correlation functions like  $C_{\mathbf{p}}(t_0, t)$  and  $C_{\mathbf{p}}(t_0, t, T)$  have been computed on the lattice (typically one computes these quantities for all possible  $t$ ), how can we extract physics from them?

### 4.2.1 Fitting Correlation Functions

Typically 2-point correlators are used to find masses and decay constants of the propagating meson. One performs a  $\chi^2$ -fit of the correlator to a theoretically motivated

function of  $t$ . To derive such a function, we use a complete set of momentum  $\mathbf{p}$  states -

$$1 = \sum_{n=0} \frac{1}{2E_n} |\lambda_n\rangle\langle\lambda_n|, \quad (4.34)$$

where  $E_n$  are the energies of each state. Inserting this into the correlation function, and moving from the Heisenberg to Schrödinger picture;

$$\begin{aligned} C_{\mathbf{p}}(t) &= \sum_{n=0} \frac{1}{2E_n} \langle \Omega | \left( e^{Ht} + e^{H(T_{\text{lat}}-t)} \right) \Phi(\mathbf{p}, 0) \left( e^{-Ht} + e^{-H(T_{\text{lat}}-t)} \right) | \lambda_n \rangle \\ &\quad \times \langle \lambda_n | \Phi^\dagger(\mathbf{p}, 0) | \Omega \rangle \\ &= \sum_{n=0} \left( \frac{\langle \Omega | \Phi(\mathbf{p}, 0) | \lambda_n \rangle}{\sqrt{2E_n}} \right) \left( \frac{\langle \lambda_n | \Phi^\dagger(\mathbf{p}, 0) | \Omega \rangle}{\sqrt{2E_n}} \right) \left( e^{-\bar{E}_n t} + e^{-\bar{E}_n (T_{\text{lat}}-t)} \right) \\ &\equiv \sum_{n=0} |a_n|^2 f(\bar{E}_n, t) \quad , \quad f(E, t) = \left( e^{-Et} + e^{-E(T_{\text{lat}}-t)} \right), \end{aligned} \quad (4.35)$$

where  $T_{\text{lat}} = aN_t$  is the temporal extent of the lattice. We have here set  $t_0 = 0$  for clarity. The fit results in a determination of the parameters  $a_n$ , and  $\bar{E}_n$ . In all of our calculations we use  $n \in [0, 5]$ . The sum over  $n$  will be populated only by states  $|\lambda_n\rangle$  with the same quantum numbers as  $\Phi$ , since  $\langle \Omega | \Phi | \lambda_n \rangle$  would vanish otherwise. We can then interpret  $|\lambda_0\rangle$  to be the ground state of the meson we are studying. The exponential decays mean the fit function is dominated by the ground state at large  $t$ , and subsequent excited states become less important as  $n$  increases. Hence by only including  $C_{\mathbf{p}}(t)$  at suitably large  $t$  values, we can afford to truncate the sum in  $n$ . In our fits we use  $n \in [0, 5]$ .

We maintain a distinction between  $\bar{E}_n$  and  $E_n$ , since for example in calculations involving NRQCD quarks these differ -  $\bar{E}_n$  is not the relativistic energy but rather goes like  $\mathbf{p}^2/2m$ .

If this is not an issue, as is the case with HISQ, one can compute the correlation function at zero momentum  $C_0(t)$ , then fit it to find the parameter  $\bar{E}_0$ , which will equal the meson's mass  $M$ .  $a_n$  can be related to the meson's decay constant. For example for a pseudoscalar meson; via the definition of a meson decay constant (2.25) and the Ward identity in (2.55), we find

$$f_M = (m_a - m_b) \sqrt{\frac{2}{M^3}} \left( \frac{a_0}{a^{3/2}} \right). \quad (4.36)$$

The above discussion can be straightforwardly generalized to 3-point correlation functions, from which we are able to extract quantities like the hadronic transition amplitudes  $\langle M' | J_\mu | M \rangle$ , from which we can determine semileptonic form factors.

The generalization of the above for 3-point correlators is

$$\begin{aligned} C_3(t, T) &= \sum_{n,m} \left( \frac{\langle 0|\Phi_{M'}|\lambda_n\rangle}{\sqrt{2E_{M,n}}} \right) \left( \frac{\langle \lambda_n|V_\mu|\lambda_m\rangle}{2\sqrt{E_{M,n}E_{M',m}}} \right) \left( \frac{\langle \lambda_m|\Phi_M^\dagger|0\rangle}{\sqrt{2E_{M,n}}} \right) \\ &\quad \times f(\bar{E}_{M',m}, T-t)f(\bar{E}_{M,n}, t) \\ &\equiv \sum_{n,m} a_{M',n} J_{nm} a_{M,m}^* f(\bar{E}_{M',m}, T-t)f(\bar{E}_{M,n}, t). \end{aligned} \quad (4.37)$$

$a_{M,n}$  will vanish for states  $|\lambda_n\rangle$  which have different quantum numbers to  $\Phi_M$ , and similarly for  $a_{M',m}$  and  $\Phi_{M'}$ . Non-zero  $a_{M,n}$ 's will match the analogous parameters extracted from fitting a 2-point function  $\langle \Phi_M^\dagger \Phi_M \rangle$ , similarly for  $a_{M',m}$ 's and  $\Phi_{M'}$ . This carries on to the energies,  $\{\bar{E}_{M,n}\}$  is the spectrum for the  $M'$  meson, and  $\{\bar{E}_{M',m}\}$  is the spectrum for the  $M$ . Therefore, we compute and fit the appropriate 2-point functions to deduce the parameters  $\{a_{M',n}\}, \{\bar{E}_{M',n}\}$ . Then, fitting  $C_{\mathbf{p}}(t, T)$  results in an accurate determination of the remaining free parameters,  $J_{nm}$ . This set contains the transition amplitude one is interested in  $\langle M'|J_\mu|M\rangle$ , recognising that

$$J_{00} = \frac{\langle M'|J_\mu|M\rangle}{2\sqrt{E^M E^{M'}}}. \quad (4.38)$$

### Oscillating States

In the case of staggered quarks, these fit functions must be modified to contain the effects of the so-called *oscillating states*. The oscillating states are the  $\zeta = (1, 0, 0, 0)$  taste. No other tastes contribute, since  $\Phi_{\mathbf{p}}$  has a 3-momentum fixed at  $\mathbf{p}$ , which we always take to be small relative to  $\pi/a$ , hence does not couple to the states at  $k \sim (0, \pi/a, 0, 0)$ ,  $k \sim (0, 0, \pi/a, 0)$  etc. However,  $\Phi_{\mathbf{p}}$  can couple to arbitrarily high energy states, so the  $k \sim (\pi/a, 0, 0, 0)$  doubler contributes. The contribution of this extra taste to  $\Phi_M = \bar{\psi}' \gamma_M \psi$  can be found by shifting it down to energies around  $\mathbf{p}$  via the doubling transform  $\psi \rightarrow (i\gamma_5 \gamma_0)(-1)^{t/a} \psi$ . So for example if  $M$  is a pseudoscalar the extra taste is  $\Phi_M \rightarrow i(-1)^{t/a} \bar{\psi} \gamma_0 \psi$ , a scalar meson with a phase  $(-1)^t/a$ .

There is a special case where oscillating states do not contribute. If the two quarks in  $\Phi_M$  are degenerate (have the same flavour, momentum etc.) then the doubling symmetry acts on both  $\psi$  and  $\psi'$ . If  $M$  is a pseudoscalar,  $\gamma_M = \gamma_5$ , then the effect of the doubling symmetry cancels, and no oscillating states contribute.

$$\bar{\psi} \gamma_5 \psi \rightarrow -(-1)^{2 \times t/a} \bar{\psi} (i\gamma_5 \gamma_0) \gamma_5 (i\gamma_5 \gamma_0) \psi = \bar{\psi} \gamma_5 \psi. \quad (4.39)$$

Accounting for oscillating states modifies the fit functions to

$$C_{\mathbf{p}}(t)|_{\text{fit}} = \sum_{j=0}^{N_{\text{exp}}} |a_j|^2 f(\bar{E}_j, t) + (-1)^{t/a} |a_{j,o}|^2 f(\bar{E}_{j,o}, t) \quad (4.40)$$

$$C_3(t, T)|_{\text{fit}} = \sum_{j,k=0}^{N_{\text{exp}}, N_{\text{exp}}} \left( a_j^M J_{jk}^{nn} a_k^{M'} f(E^{H_s}, t) f(E_n^{M'}, T-t) \right. \quad (4.41)$$

$$\begin{aligned} &+ a_j^{M,o} J_{jk}^{on} a_k^{M'} (-1)^t f(E_n^{M,o}, t) f(E^{M'}, T-t) \\ &+ a_j^M J_{jk}^{no} a_k^{M',o} (-1)^{T-t} f(E^M, t) f(E_n^{M',o}, T-t) \\ &\left. + a_j^{M,o} J_{jk}^{oo} a_k^{M',o} (-1)^T f(E_n^{M,o}, t) f(E^{M',o}, T-t) \right). \end{aligned} \quad (4.42)$$

We use the **CorrFitter** package [94] for performing Bayesian least-squares fitting to the correlation functions. The package employs the trust region method of least-squares fitting. The Bayesian approach, including the formalism used to set priors for the fits, was introduced in [95].

### 4.2.2 Signal Degredation

A large obstacle in the analysis of correlation functions is the *signal degredation* of correlation functions computed on the lattice.

A random variable  $x$  has a mean and standard deviation

$$\hat{x} = \langle x \rangle, \quad \sigma^2 = \frac{1}{N} (\langle x^2 \rangle - \langle x \rangle^2), \quad (4.43)$$

where  $N$  is the size of the sample. So the (square of) the signal/noise ratio is

$$\frac{\hat{x}^2}{\sigma^2} = N \left( \frac{\langle x^2 \rangle}{\langle x \rangle^2} - 1 \right)^{-1}. \quad (4.44)$$

Consider 2 point correlators where  $x = \Phi^\dagger(t)\Phi(0)$ , where  $\Phi$  is some meson operator.

$\langle x^2 \rangle$  and  $\langle x \rangle$  can be written as

$$\langle x \rangle = \sum_n \frac{1}{2E_n} \langle 0 | \Phi^\dagger(t) | \lambda_n \rangle \langle \lambda_n | \Phi(0) | 0 \rangle e^{-E_n t} \xrightarrow{t \rightarrow \infty} e^{-E_0 t}, \quad (4.45)$$

$$\langle x^2 \rangle = \sum_n \frac{1}{2E_n} \langle 0 | \Phi^{\dagger 2}(t) | \lambda_n \rangle \langle \lambda_n | \Phi^2(0) | 0 \rangle e^{-E_n t} \xrightarrow{t \rightarrow \infty} e^{-E'_0 t}. \quad (4.46)$$

where we have assumed the ratio of matrix elements and energies are  $\mathcal{O}(1)$ . The two ground state energies  $E_0$  and  $E'_0$  need not be the same, since the lowest states for which  $\langle \lambda_n | \Phi(0) | 0 \rangle \neq 0$  and  $\langle \lambda_n | \Phi^2(0) | 0 \rangle \neq 0$  may differ.

The operator  $\Phi^2$  will contain two quark and two antiquark operators, connected by some matrices in spin space.  $\Phi^2$  can create a combination of all possible 2 meson

states where the mesons are made of the available quark species, and quantum numbers. For example, for 2-point  $D$ -meson correlators ( $c\bar{d}$  pseudoscalars),  $E'_0 = (M_\pi + M_{\eta_c})$ . Plugging  $E_0 = M_{D_s}$  and this  $E'_0$  expression into (4.45),(4.46) and (4.44), we see that  $D$  meson correlators have a signal/noise ratio that degrades like

$$\frac{\hat{x}^2}{\sigma^2} \propto e^{-(M_D - (M_\pi + M_{\eta_c})/2)t}. \quad (4.47)$$

In general, a meson with two valence quarks of very different masses will suffer from this problem.  $B$ -mesons suffer more than  $D$ -mesons. Adding spacial momentum to one of the quarks in the meson would have the effect of replacing  $M_D$  in the above equation with some higher energy  $E_D$ , thus exacerbating the problem further.

### 4.3 Renormalization of Currents

Once one has computed an observable on the lattice, like  $f_M$  or  $\langle M'|J_\mu|M\rangle$ , it needs to be translated into a continuum regularization scheme. Suppose we have some bare operator  $\mathcal{O}_0$ , we expect this to be related to the renormalized operator in  $\overline{MS}$  at scale  $\mu$ ,  $\mathcal{O}^{\overline{MS}}(\mu)$ , via

$$\mathcal{O}^{\overline{MS}}(\mu) = Z^{\overline{MS}}(\mu)\mathcal{O}_0. \quad (4.48)$$

Similarly, in a lattice regularization,

$$\mathcal{O}^{\text{lat}}(1/a) = Z^{\text{lat}}(1/a)\mathcal{O}_0. \quad (4.49)$$

Hence we expect a multiplicative factor between the lattice matrix elements, and the continuum  $\overline{MS}$  ones:

$$\langle \mathcal{O} \rangle^{\overline{MS}} = \mathcal{Z}(\mu, 1/a)\langle \mathcal{O} \rangle^{\text{lat}} \quad (4.50)$$

where  $\mathcal{Z}(\mu, 1/a) = Z^{\overline{MS}}(\mu)/Z^{\text{lat}}(1/a)$ . These “matching factors”  $\mathcal{Z}$  can be deduced by equating observables calculated in both lattice QCD and continuum (appropriately regularized) QCD, producing equations which can be solved for  $\mathcal{Z}$ . The lattice side of the calculation can be done either through lattice perturbation theory (*perturbative matching*), or through a lattice calculation (*non-perturbative matching*).

The result that conserved (or partially conserved) currents (and densities connected to those currents via Ward identities) do not receive any renormalization in any scheme, i.e.  $Z^{\text{any}} = 1$ . They are said to be *absolutely normalized*.

In principle this is of great help, since the currents that mediate semileptonic decays, e.g. the weak vector and axial currents, are partially conserved, so we are not required to include any matching factors. However, in practice, this is complicated by the fact that the conserved current in the lattice theory is often computationally difficult or impossible to compute. For example, in NRQCD, the partially conserved current corresponding to  $SU(N)_V$  is an infinite sum in  $1/m_b$  where  $m_b$  is the bottom mass. The corresponding current in HISQ is also the sum of a large number of operators. This can be interpreted as a mixing in the renormalization:

$$\langle \mathcal{O}_i \rangle^{\overline{MS}} = \mathcal{Z}_{i,j} \langle \mathcal{O}_j \rangle^{\text{lat}} \quad (4.51)$$

Lattice calculations often use only the dominant operators that contribute to the conserved current. Since these will be “close” to the conserved current, one can expect the matching factor to only be a small deviation from unity, and the more sub-dominant operators you add, the overall matching factor should tend towards unity.

## CHAPTER 5

# $b$ -Physics from Lattice NRQCD

---

### 5.1 $B_{(s)} \rightarrow D_{(s)} l \nu$ Form Factors

brief motivation

disclaimer: this was never properly finished! (is it ok to say this?)

#### 5.1.1 Calculation Setup

ensemble details, what correlators were calculated, etc.

#### 5.1.2 Results

as far as I got : plots of form factors

discuss how too many correlators makes the fits very unstable...

#### 5.1.3 The Subleading Current Problem

Talk about the fact that  $J_k^{(3,4)}$  are huge, how there isn't much way around this

### 5.2 Nonperturbative Renormalisation

#### 5.2.1 Relativistic Normalisation of the $b \rightarrow c$ Axial Current

brief description of what we were trying to do: test normalisations, or fix new normalisations

results - plots of  $a_0(p)/a_0(0)$  against  $p^2$

why it didn't work

#### 5.2.2 $b \rightarrow c$ Vector Current Matching to Heavy-HISQ

Explain that  $B_c \rightarrow \eta_c$  data from both heavy-HISQ and NRQCD were available, ref. Andrew & Brian.

Fix normalisation of  $V_0$  by comparing  $f_0/f_{B_c}$  at zero recoil at  $q^2 = 0$ .



## CHAPTER 6

# $B_s \rightarrow D_s^* l \nu$ Axial Form Factor at Zero Recoil from Heavy-HISQ

---

brief motivation,  $V_{cb}$  etc.

## 6.1 Calculation Setup

ensembles, masses, etc. used

basically going to repurpose paper in here

## 6.2 Results

## 6.3 Implications for $B \rightarrow D^* l \nu$ and $|V_{cb}|$

$B \rightarrow D^*$ , fermilab data plot, how it relates to  $|V_{cb}|$  tensions etc.



## CHAPTER 7

# $B_s \rightarrow D_s l \nu$ Form Factor at All Physical $q^2$ from Heavy-HISQ

---

brief motivation,  $V_{cb}$  etc.

## 7.1 Calculation Setup

basically repurpose paper again

## 7.2 Results

## 7.3 HQET low energy constants

won't mention this in the paper, but i did some work fitting  $h_+$  to the HQET expression, similar to in the  $Bs - Ds^*$  case



# List of Figures

2.1	The flavour-changing charged current vertex. . . . .	8
2.2	A sketch of the unitarity triangle. . . . .	9
2.3	Exclusion regions for the vertices of the CKM triangle from various measurements, courtesy of the most recent PDG update [1]. . . . .	10
2.4	Leptonic decay of meson $M$ at tree level in the electroweak coupling. . . . .	11
2.5	Semileptonic decay, $M \rightarrow M' l \bar{\nu}$ , at tree level in electroweak coupling. . . . .	12
2.6	Different determinations of $ V_{cb} $ . Points labelled $w = 1$ are determinations from extrapolating measurements of decay rates to the zero recoil point, and combining them with a lattice determination of the form factor at zero recoil. Points labelled $w \geq 1$ are results from using a combination of both branching fractions and lattice form factors through some range of $w$ . The first name mentioned in the labels give the source of the lattice form factors, and the second gives the source of the experimental data (e.g. the HPQCD+BaBar point used form factors from the HPQCD collaboration and data from the BaBar experiment). The highest point is from [6], the second and third highest from [7], fourth from [8], fifth from [9]. The bottom point is from the PDG [1], using data from the ALPEPH [10], Belle [11], BaBar [12,13], and CLEO [14] experiments. . . . .	15
2.7	$R(D^{(*)})$ determinations from SM and measurement [27] . . . . .	17
2.8	The relationship between scale $Q$ and the strong coupling constant $\alpha_s$ , from the PDG [1]. . . . .	20
3.1	Depiction of colour spaces (fibres) at two points in spactime (base space) with the value of the quark field $q$ represented at each point as a colour vector, and the connection $W(x, y)$ needed to compare the two colour vectors. A gauge transform changes the two vectors in different ways, for the comparison to be gauge independent, the connection must also transform appropriately. . . . .	32
3.2	Depiction of a gauge invariant quark bilinear, connected by a Wilson line made of gauge links. . . . .	32
3.3	Elementary Plaquette. . . . .	33

3.4	Terms additional to the elementary plaquette in the improved pure QCD action. . . . .	35
3.5	Taste mixing at tree level. . . . .	40
3.6	Different scales relevant to non-perturbative physics, and brackets showing the range of scales that typical lattices can resolve. The larger the range of scales resolved, the more computationally expensive the calculation. . . . .	42
3.7	An extrapolation to $m_h = m_b$ of the $\eta_h$ decay constant (where $\eta_h$ is a pseudoscalar $\bar{h}h$ meson [69]. The colourful points are measurements of $f_{\eta_h}$ on the lattice, the colour denotes lattice spacing. The $x$ axis, $M_{\eta_h}$ , is a proxy for the $h$ -quark mass. . . . .	43

# List of Tables

- 4.1 Parameters for gluon ensembles [88, 89].  $a$  values for sets 0-3 were deduced in [90], set 4 from [91]. We thank C. McNeile for computing the  $a$  value on set 5. These  $a$  values are determined by measuring the Wilson flow parameter  $w_0/a$  on the lattice, then using the known value for  $w_0$  to isolate  $a$ . Columns 5-7 give the masses used in the action for light, strange and charm quarks in the sea. . . . . 52



# Bibliography

- [1] M. et. al. Tanabashi. Review of particle physics. *Phys. Rev. D*, 98:030001, Aug 2018.
- [2] Bugra Borasoy. Introduction to Chiral Perturbation Theory. *Springer Proc. Phys.*, 118:1–26, 2008.
- [3] Bernard Aubert et al. Measurements of the  $B \rightarrow D^*$  form-factors using the decay  $\bar{B}^0 \rightarrow D^{*+} e^-$  electron-neutrino. *Phys. Rev.*, D74:092004, 2006.
- [4] Ikaros I. Y. Bigi, Mikhail A. Shifman, N. Uraltsev, and Arkady I. Vainshtein. High power  $n$  of  $m_b$  in beauty widths and  $n = 5 \rightarrow \infty$  limit. *Phys. Rev.*, D56:4017–4030, 1997. [,205(1996)].
- [5] Andre H. Hoang, Zoltan Ligeti, and Aneesh V. Manohar.  $B$  decays in the upsilon expansion. *Phys. Rev.*, D59:074017, 1999.
- [6] Heechang Na, Chris M. Bouchard, G. Peter Lepage, Chris Monahan, and Junko Shigemitsu.  $B \rightarrow Dl\nu$  form factors at nonzero recoil and extraction of  $|V_{cb}|$ . *Phys. Rev.*, D92(5):054510, 2015. [Erratum: *Phys. Rev.*D93,no.11,119906(2016)].
- [7] Jon A. Bailey et al.  $B \rightarrow Dl\nu$  form factors at nonzero recoil and  $|V_{cb}|$  from 2+1-flavor lattice QCD. *Phys. Rev.*, D92(3):034506, 2015.
- [8] Jon A. Bailey et al. Update of  $|V_{cb}|$  from the  $\bar{B} \rightarrow D^*\ell\bar{\nu}$  form factor at zero recoil with three-flavor lattice QCD. *Phys. Rev.*, D89(11):114504, 2014.
- [9] Benjamin Grinstein and Andrew Kobach. Model-Independent Extraction of  $|V_{cb}|$  from  $\bar{B} \rightarrow D^*\ell\bar{\nu}$ . *Phys. Lett.*, B771:359–364, 2017.
- [10] D Buskulic et. al. A measurement of  $|v_{cb}|$  from  $b^0 \rightarrow d^* l^- \nu_l$ . *Physics Letters B*, 359(1):236 – 248, 1995.
- [11] Kazuo Abe et al. Measurement of  $B(\text{anti-}B^0 \rightarrow D^+ l^- \text{anti-}\nu_l)$  and determination of  $|V(cb)|$ . *Phys. Lett.*, B526:258–268, 2002.
- [12] Bernard Aubert et al. Measurements of the Semileptonic Decays  $\text{anti-}B \rightarrow D l \text{ anti-}\nu_l$  and  $\text{anti-}B \rightarrow D^* l \text{ anti-}\nu_l$  Using a Global Fit to  $D \times l \text{ anti-}\nu_l$  Final States. *Phys. Rev.*, D79:012002, 2009.

- [13] Bernard Aubert et al. Measurement of  $|V(cb)|$  and the Form-Factor Slope in  $B \rightarrow D l^- \bar{\nu}_l$  Decays in Events Tagged by a Fully Reconstructed  $B$  Meson. *Phys. Rev. Lett.*, 104:011802, 2010.
- [14] John E. Bartelt et al. Measurement of the  $B \rightarrow D$  lepton neutrino branching fractions and form-factor. *Phys. Rev. Lett.*, 82:3746, 1999.
- [15] Dante Bigi, Paolo Gambino, and Stefan Schacht. A fresh look at the determination of  $|V_{cb}|$  from  $B \rightarrow D^* \ell \bar{\nu}$ . *Phys. Lett.*, B769:441–445, 2017.
- [16] Jon A. Bailey, Sunkyu Lee, Weonjong Lee, Jaehoon Leem, and Sungwoo Park. Updated evaluation of  $\epsilon_K$  in the standard model with lattice QCD inputs. *Phys. Rev.*, D98(9):094505, 2018.
- [17] J. P. Lees et al. Evidence for an excess of  $\bar{B} \rightarrow D^{(*)} \tau^- \bar{\nu}_\tau$  decays. *Phys. Rev. Lett.*, 109:101802, 2012.
- [18] J. P. Lees et al. Measurement of an Excess of  $\bar{B} \rightarrow D^{(*)} \tau^- \bar{\nu}_\tau$  Decays and Implications for Charged Higgs Bosons. *Phys. Rev.*, D88(7):072012, 2013.
- [19] M. Huschle et al. Measurement of the branching ratio of  $\bar{B} \rightarrow D^{(*)} \tau^- \bar{\nu}_\tau$  relative to  $\bar{B} \rightarrow D^{(*)} \ell^- \bar{\nu}_\ell$  decays with hadronic tagging at Belle. *Phys. Rev.*, D92(7):072014, 2015.
- [20] Y. Sato et al. Measurement of the branching ratio of  $\bar{B}^0 \rightarrow D^{*+} \tau^- \bar{\nu}_\tau$  relative to  $\bar{B}^0 \rightarrow D^{*+} \ell^- \bar{\nu}_\ell$  decays with a semileptonic tagging method. *Phys. Rev.*, D94(7):072007, 2016.
- [21] S. Hirose et al. Measurement of the  $\tau$  lepton polarization and  $R(D^*)$  in the decay  $\bar{B} \rightarrow D^* \tau^- \bar{\nu}_\tau$ . *Phys. Rev. Lett.*, 118(21):211801, 2017.
- [22] S. Hirose et al. Measurement of the  $\tau$  lepton polarization and  $R(D^*)$  in the decay  $\bar{B} \rightarrow D^* \tau^- \bar{\nu}_\tau$  with one-prong hadronic  $\tau$  decays at Belle. *Phys. Rev.*, D97(1):012004, 2018.
- [23] Roel Aaij et al. Measurement of the ratio of branching fractions  $\mathcal{B}(\bar{B}^0 \rightarrow D^{*+} \tau^- \bar{\nu}_\tau) / \mathcal{B}(\bar{B}^0 \rightarrow D^{*+} \mu^- \bar{\nu}_\mu)$ . *Phys. Rev. Lett.*, 115(11):111803, 2015. [Erratum: Phys. Rev. Lett. 115, no. 15, 159901 (2015)].
- [24] R. Aaij et al. Measurement of the ratio of the  $B^0 \rightarrow D^{*-} \tau^+ \nu_\tau$  and  $B^0 \rightarrow D^{*-} \mu^+ \nu_\mu$  branching fractions using three-prong  $\tau$ -lepton decays. *Phys. Rev. Lett.*, 120(17):171802, 2018.

- [25] R. Aaij et al. Test of Lepton Flavor Universality by the measurement of the  $B^0 \rightarrow D^{*-} \tau^+ \nu_\tau$  branching fraction using three-prong  $\tau$  decays. *Phys. Rev.*, D97(7):072013, 2018.
- [26] Svjetlana Fajfer, Jernej F. Kamenik, and Ivan Nisandzic. On the  $B \rightarrow D^* \tau \bar{\nu}_\tau$  Sensitivity to New Physics. *Phys. Rev.*, D85:094025, 2012.
- [27] Y. Amhis et al. Averages of  $b$ -hadron,  $c$ -hadron, and  $\tau$ -lepton properties as of summer 2016. *Eur. Phys. J.*, C77:895, 2017. updated results and plots available at <https://hflav.web.cern.chhttps://hflav.web.cern.ch>.
- [28] Wolfgang Altmannshofer, Peter Stangl, and David M. Straub. Interpreting Hints for Lepton Flavor Universality Violation. *Phys. Rev.*, D96(5):055008, 2017.
- [29] Christoph Bobeth, Gudrun Hiller, and Giorgi Piranishvili. Angular distributions of  $\bar{B} \rightarrow \bar{K} \ell^+ \ell^-$  decays. *JHEP*, 12:040, 2007.
- [30] Chris Bouchard, G. Peter Lepage, Christopher Monahan, Heechang Na, and Junko Shigemitsu. Standard Model Predictions for  $B \rightarrow K \ell^+ \ell^-$  with Form Factors from Lattice QCD. *Phys. Rev. Lett.*, 111(16):162002, 2013. [Erratum: *Phys. Rev. Lett.* 112,no.14,149902(2014)].
- [31] Roel Aaij et al. Test of lepton universality using  $B^+ \rightarrow K^+ \ell^+ \ell^-$  decays. *Phys. Rev. Lett.*, 113:151601, 2014.
- [32] Marzia Bordone, Gino Isidori, and Andrea Patti. On the Standard Model predictions for  $R_K$  and  $R_{K^*}$ . *Eur. Phys. J.*, C76(8):440, 2016.
- [33] Sébastien Descotes-Genon, Lars Hofer, Joaquim Matias, and Javier Virto. Global analysis of  $b \rightarrow s \ell \ell$  anomalies. *JHEP*, 06:092, 2016.
- [34] Bernat Capdevila, Sébastien Descotes-Genon, Joaquim Matias, and Javier Virto. Assessing lepton-flavour non-universality from  $B \rightarrow K^* \ell \ell$  angular analyses. *JHEP*, 10:075, 2016.
- [35] Bernat Capdevila, Sébastien Descotes-Genon, Lars Hofer, and Joaquim Matias. Hadronic uncertainties in  $B \rightarrow K^* \mu^+ \mu^-$ : a state-of-the-art analysis. *JHEP*, 04:016, 2017.

- [36] Nicola Serra, Rafael Silva Coutinho, and Danny van Dyk. Measuring the breaking of lepton flavor universality in  $B \rightarrow K^* \ell^+ \ell^-$ . *Phys. Rev.*, D95(3):035029, 2017.
- [37] Aoife Bharucha, David M. Straub, and Roman Zwicky.  $B \rightarrow V \ell^+ \ell^-$  in the Standard Model from light-cone sum rules. *JHEP*, 08:098, 2016.
- [38] Wolfgang Altmannshofer, Christoph Niehoff, Peter Stangl, and David M. Straub. Status of the  $B \rightarrow K^* \mu^+ \mu^-$  anomaly after Moriond 2017. *Eur. Phys. J.*, C77(6):377, 2017.
- [39] Sebastian Jäger and Jorge Martin Camalich. Reassessing the discovery potential of the  $B \rightarrow K^* \ell^+ \ell^-$  decays in the large-recoil region: SM challenges and BSM opportunities. *Phys. Rev.*, D93(1):014028, 2016.
- [40] R. Aaij et al. Test of lepton universality with  $B^0 \rightarrow K^{*0} \ell^+ \ell^-$  decays. *JHEP*, 08:055, 2017.
- [41] Kazuo Abe et al. An Upper bound on the decay tau —> mu gamma from Belle. *Phys. Rev. Lett.*, 92:171802, 2004.
- [42] A. M. Baldini et al. Search for the lepton flavour violating decay  $\mu^+ \rightarrow e^+ \gamma$  with the full dataset of the MEG experiment. *Eur. Phys. J.*, C76(8):434, 2016.
- [43] Marat Freytsis, Zoltan Ligeti, and Joshua T. Ruderman. Flavor models for  $\bar{B} \rightarrow D^{(*)} \tau \bar{\nu}$ . *Phys. Rev.*, D92(5):054018, 2015.
- [44] Martin Bauer and Matthias Neubert. Minimal Leptoquark Explanation for the  $R_{D^{(*)}}$ ,  $R_K$ , and  $(g-2)_g$  Anomalies. *Phys. Rev. Lett.*, 116(14):141802, 2016.
- [45] Andreas Crivellin, Giancarlo D'Ambrosio, and Julian Heeck. Explaining  $h \rightarrow \mu^\pm \tau^\mp$ ,  $B \rightarrow K^* \mu^+ \mu^-$  and  $B \rightarrow K \mu^+ \mu^- / B \rightarrow K e^+ e^-$  in a two-Higgs-doublet model with gauged  $L_\mu - L_\tau$ . *Phys. Rev. Lett.*, 114:151801, 2015.
- [46] Matthew D. Schwartz. *Quantum Field Theory and the Standard Model*. Cambridge University Press, 2014.
- [47] I.S. Altarev, Yu.V. Borisov, N.V. Borovikova, S.N. Ivanov, E.A. Kolomensky, M.S. Lasakov, V.M. Lobashev, V.A. Nazarenko, A.N. Pirozhkov, A.P. Serebrov, Yu.V. Sobolev, E.V. Shulgina, and A.I. Yegorov. New measurement of the electric dipole moment of the neutron. *Physics Letters B*, 276(1):242 – 246, 1992.

- [48] David J. Gross and Frank Wilczek. Ultraviolet behavior of non-abelian gauge theories. *Phys. Rev. Lett.*, 30:1343–1346, Jun 1973.
- [49] Stefan Scherer. Introduction to chiral perturbation theory. *Adv. Nucl. Phys.*, 27:277, 2003. [,277(2002)].
- [50] S. Fubini and G. Furlan. Renormalization effects for partially conserved currents. *Physics Physique Fizika*, 1(4):229–247, 1965.
- [51] Richard F. Lebed and Mahiko Suzuki. Current algebra and the Ademollo-Gatto theorem in spin flavor symmetry of heavy quarks. *Phys. Rev.*, D44:829–836, 1991.
- [52] Leslie L. Foldy and Siegfried A. Wouthuysen. On the dirac theory of spin 1/2 particles and its non-relativistic limit. *Phys. Rev.*, 78:29–36, Apr 1950.
- [53] G. Peter Lepage, Lorenzo Magnea, Charles Nakhleh, Ulrika Magnea, and Kent Hornbostel. Improved nonrelativistic QCD for heavy quark physics. *Phys. Rev.*, D46:4052–4067, 1992.
- [54] Philippe de Forcrand. Simulating QCD at finite density. *PoS*, LAT2009:010, 2009.
- [55] M. Lüscher and P. Weisz. On-shell improved lattice gauge theories. *Comm. Math. Phys.*, 97(1-2):59–77, 1985.
- [56] P. Weisz. Continuum limit improved lattice action for pure yang-mills theory (i). *Nuclear Physics B*, 212(1):1 – 17, 1983.
- [57] P. Weisz and R. Wohlert. Continuum limit improved lattice action for pure yang-mills theory (ii). *Nuclear Physics B*, 236(2):397 – 422, 1984.
- [58] A. Hart, G. M. von Hippel, and R. R. Horgan. Radiative corrections to the lattice gluon action for HISQ improved staggered quarks and the effect of such corrections on the static potential. *Phys. Rev.*, D79:074008, 2009.
- [59] Kenneth G. Wilson. Confinement of Quarks. *Phys. Rev.*, D10:2445–2459, 1974. [,319(1974)].
- [60] John B. Kogut and Leonard Susskind. Hamiltonian Formulation of Wilson’s Lattice Gauge Theories. *Phys. Rev.*, D11:395–408, 1975.

- [61] E. Follana, Q. Mason, C. Davies, K. Hornbostel, G. P. Lepage, J. Shigemitsu, H. Trottier, and K. Wong. Highly improved staggered quarks on the lattice, with applications to charm physics. *Phys. Rev.*, D75:054502, 2007.
- [62] C. T. H. Davies et al. Precision charm physics, m(c) and alpha(s) from lattice QCD. *PoS*, LATTICE2008:118, 2008.
- [63] C. T. H. Davies. Precision charmonium and D physics from lattice QCD and determination of the charm quark mass. In *Proceedings, 34th International Conference on High Energy Physics (ICHEP 2008): Philadelphia, Pennsylvania, July 30-August 5, 2008*, 2008.
- [64] Jonna Koponen, Christine T. H. Davies, Gordon Donald, Eduardo Follana, G. Peter Lepage, Heechang Na, and Junko Shigemitsu. The D to K and D to pi semileptonic decay form factors from Lattice QCD. *PoS*, LATTICE2011:286, 2011.
- [65] Heechang Na, Christine T. H. Davies, Eduardo Follana, Jonna Koponen, G. Peter Lepage, and Junko Shigemitsu.  $D \rightarrow \pi, l\nu$  Semileptonic Decays,  $|V_{cd}|$  and 2<sup>nd</sup> Row Unitarity from Lattice QCD. *Phys. Rev.*, D84:114505, 2011.
- [66] Heechang Na, Chris Monahan, Christine Davies, Eduardo Follana, Ron Horgan, Peter Lepage, and Junko Shigemitsu. Precise Determinations of the Decay Constants of B and D mesons. *PoS*, LATTICE2012:102, 2012.
- [67] Heechang Na, Christine T. H. Davies, Eduardo Follana, G. Peter Lepage, and Junko Shigemitsu.  $|V_{cd}|$  from D Meson Leptonic Decays. *Phys. Rev.*, D86:054510, 2012.
- [68] Jonna Koponen. Lattice results for  $D/D_s$  leptonic and semileptonic decays. In *Proceedings, 6th International Workshop on Charm Physics (Charm 2013): Manchester, UK, August 31-September 4, 2013*, 2013.
- [69] C. McNeile, C. T. H. Davies, E. Follana, K. Hornbostel, and G. P. Lepage. Heavy meson masses and decay constants from relativistic heavy quarks in full lattice QCD. *Phys. Rev.*, D86:074503, 2012.
- [70] Andrew Lytle, Brian Colquhoun, Christine Davies, Jonna Koponen, and Craig McNeile. Semileptonic  $B_c$  decays from full lattice QCD. *PoS*, BEAUTY2016:069, 2016.

- [71] A. Gray, I. Allison, C. T. H. Davies, Emel Dalgic, G. P. Lepage, J. Shigemitsu, and M. Wingate. The Upsilon spectrum and m(b) from full lattice QCD. *Phys. Rev.*, D72:094507, 2005.
- [72] Christine T. H. Davies, Judd Harrison, Ciaran Hughes, Ronald R. Horgan, Georg M. von Hippel, and Matthew Wingate. Improving the Kinetic Couplings in Lattice Non-Relativistic QCD. 2018.
- [73] R. J. Dowdall et al. The Upsilon spectrum and the determination of the lattice spacing from lattice QCD including charm quarks in the sea. *Phys. Rev.*, D85:054509, 2012.
- [74] Michael E. Peskin and Daniel V. Schroeder. *An Introduction to quantum field theory*. 1995.
- [75] David J. E. Callaway and Aneesur Rahman. Microcanonical ensemble formulation of lattice gauge theory. *Phys. Rev. Lett.*, 49:613–616, Aug 1982.
- [76] David J. E. Callaway and Aneesur Rahman. Lattice gauge theory in the microcanonical ensemble. *Phys. Rev. D*, 28:1506–1514, Sep 1983.
- [77] Simon Duane and John B. Kogut. Hybrid stochastic differential equations applied to quantum chromodynamics. *Phys. Rev. Lett.*, 55:2774–2777, Dec 1985.
- [78] Simon Duane and John Kogut. The theory of hybrid stochastic algorithms. *Nuclear Physics B*, 275:398–420, 11 1986.
- [79] Nicholas Metropolis, Arianna W. Rosenbluth, Marshall N. Rosenbluth, Augusta H. Teller, and Edward Teller. Equation of state calculations by fast computing machines. *The Journal of Chemical Physics*, 21(6):1087–1092, 1953.
- [80] Simon Duane, A.D. Kennedy, Brian J. Pendleton, and Duncan Roweth. Hybrid monte carlo. *Physics Letters B*, 195(2):216 – 222, 1987.
- [81] Steven Gottlieb, W. Liu, D. Toussaint, R. L. Renken, and R. L. Sugar. Hybrid-molecular-dynamics algorithms for the numerical simulation of quantum chromodynamics. *Phys. Rev. D*, 35:2531–2542, Apr 1987.
- [82] K. Jansen. Actions for dynamical fermion simulations: are we ready to go? *Nuclear Physics B - Proceedings Supplements*, 129-130:3 – 16, 2004. Lattice 2003.

- [83] Michael Creutz. Chiral anomalies and rooted staggered fermions. *Physics Letters B*, 649(2):230 – 234, 2007.
- [84] Michael Creutz. Why rooting fails. *PoS*, LATTICE2007:007, 2007.
- [85] M. A. Clark and A. D. Kennedy. Accelerating dynamical fermion computations using the rational hybrid Monte Carlo (RHMC) algorithm with multiple pseudofermion fields. *Phys. Rev. Lett.*, 98:051601, 2007.
- [86] Andreas Frommer, Bertold Nockel, Stephan Gusken, Thomas Lippert, and Klaus Schilling. Many masses on one stroke: Economic computation of quark propagators. *Int. J. Mod. Phys.*, C6:627–638, 1995.
- [87] Beat Jegerlehner. Krylov space solvers for shifted linear systems. 1996.
- [88] A. Bazavov et al. Lattice QCD ensembles with four flavors of highly improved staggered quarks. *Phys. Rev.*, D87(5):054505, 2013.
- [89] A. Bazavov et al. Scaling studies of QCD with the dynamical HISQ action. *Phys. Rev.*, D82:074501, 2010.
- [90] R. J. Dowdall, C. T. H. Davies, G. P. Lepage, and C. McNeile. Vus from pi and K decay constants in full lattice QCD with physical u, d, s and c quarks. *Phys. Rev.*, D88:074504, 2013.
- [91] Bipasha Chakraborty, C. T. H. Davies, B. Galloway, P. Knecht, J. Koponen, G. C. Donald, R. J. Dowdall, G. P. Lepage, and C. McNeile. High-precision quark masses and QCD coupling from  $n_f = 4$  lattice QCD. *Phys. Rev.*, D91(5):054508, 2015.
- [92] M. R. Hestenes and E. Stiefel. Methods of conjugate gradients for solving linear systems. *Journal of research of the National Bureau of Standards*, 49:409–436, 1952.
- [93] D. Guadagnoli, F. Mescia, and S. Simula. Lattice study of semileptonic form-factors with twisted boundary conditions. *Phys. Rev.*, D73:114504, 2006.
- [94] G.P.Lepage. Corrfitter: <https://github.com/gplepage/corrfitter>, 2012.
- [95] G. P. Lepage, B. Clark, C. T. H. Davies, K. Hornbostel, P. B. Mackenzie, C. Morningstar, and H. Trottier. Constrained curve fitting. *Nucl. Phys. Proc. Suppl.*, 106:12–20, 2002. [,12(2001)].